Available online at www.sciencedirect.com

ScienceDirect

Geochimica et Cosmochimica Acta 268 (2020) 1–21

Geochimica et Cosmochimica Acta

www.elsevier.com/locate/gca

Multi-elemental composition of authigenic carbonates in benthic foraminifera from the eastern Bering Sea continental margin (International Ocean Discovery Program Site U1343)

Henrieka Detlef [a,*], Sindia M. Sosdian [a], Sev Kender [b,c], Caroline H. Lear [a], Ian R. Hall [a]

[a] School of Earth and Ocean Sciences, Cardiff University, Main Building, Park Place, Cardiff CF10 3AT, UK
[b] University of Exeter, Camborne School of Mines, Penryn, Cornwall TR10 9FE, UK
[c] British Geological Survey Keyworth, Nottingham NG12 5GG, UK

Received 22 January 2019; accepted in revised form 11 September 2019; Available online 21 September 2019

Abstract

Bering Sea sediments represent exceptional archives, offering the potential to study past climates and biogeochemistry at a high resolution. However, abundant hydrocarbons of microbial origin, especially along the eastern Bering Sea continental margin, can hinder the applicability of palaeoceanographic proxies based on calcareous foraminifera, due to the formation of authigenic carbonates. Nonetheless, authigenic carbonates may also bear unique opportunities to reconstruct changes in the sedimentary redox environment.

Here we use a suite of visual and geochemical evidence from single-specimens of the shallow infaunal benthic foraminiferal species *Elphidium batialis* Saidova (1961), recovered from International Ocean Discovery Program (IODP) Site U1343 in the eastern Bering Sea, to investigate the influence of authigenic carbonates on the foraminiferal trace metal composition. Our results demonstrate that foraminiferal calcite tests act as a nucleation template for secondary carbonate precipitation, altering their geochemistry where organoclastic sulphate reduction and anaerobic oxidation of methane cause the formation of low- and high-Mg calcite, respectively. The authigenic carbonates can occur as encrusting on the outside and/or inside of foraminiferal tests, in the form of recrystallization of the test wall, or as banding along natural laminations within the foraminiferal test walls. In addition to Mg, authigenic carbonates are enriched in U/Ca, Mn/Ca, Fe/Ca, and Sr/Ca, depending on the redox environment that they were formed in. Our results demonstrate that site-specific U/Ca thresholds are a promising tool to distinguish between diagenetically altered and pristine foraminiferal samples, important for palaeoceanographic reconstructions utilising the primary foraminiferal geochemistry. Consistent with previous studies, U/Mn ratios of foraminifera at IODP Site U1343 increase according to their degree of diagenetic alteration, suggesting a potential response of authigenic U/Mn to the microbial activity in turn linked to the sedimentary redox environment.

Keywords: Foraminifera; Diagenesis; Foraminiferal trace metals; Continental margins; Methane; Laser inductively coupled plasma mass spectrometry; Electron probe microanalysis; Scanning electron microscopy

Abbreviations: IODP, international ocean discovery program; HNLC, high nutrient low chlorophyll; OMZ, oxygen minimum zone; BWT, bottom water temperature; mbsf, meters below seafloor; LMC, low-Mg calcite; HMC, high-Mg calcite; CCSF-A, core composite depth below seafloor; MR, medium resolution; LR, low resolution; LOD, limit of detection; CI, confidence interval; s.d., standard deviation.

* Corresponding author at: Department of Geoscience, Aarhus University, Høegh-Guldbergs Gade 2, 8000 Aarhus C, Denmark.
E-mail address: henrieka.detlef@geo.au.dk (H. Detlef).

https://doi.org/10.1016/j.gca.2019.09.025
0016-7037/

1. INTRODUCTION

As part of the International Ocean Discovery Program (IODP) Expedition 323 several locations were cored along the eastern Bering Sea continental margin, with high siliciclastic and organoclastic sedimentation rates indicating the opportunity to study Quaternary climates at a sub-orbital resolution. Available palaeoceanographic reconstructions at IODP Site U1343 (Kim et al., 2014; Asahi et al., 2016; Detlef et al., 2018; Kender et al., 2018) (57°33.4′N, 176° 49.0′W; 1953 m water depth) (Fig. 1) demonstrate its potential to provide millennial scale climate and biogeochemical archives. Thus, the elemental and isotopic composition of planktonic and benthic foraminifera at IODP Site U1343 could provide an unrivalled record of climate variability in a region from which there is currently a dearth of information (Kender et al., 2018). However, the report of co-occurrence of discoloured foraminiferal tests with authigenic carbonate crystals within the sediments of IODP Site U1343 (Expedition 323 Scientists, 2010), indicates the necessity to examine the potential influence of sedimentary diagenesis on foraminiferal geochemistry before this archive is fully utilised.

Previous work on planktonic and benthic foraminifera in pelagic and hemi-pelagic settings has shown that post-mortem interactions of foraminiferal calcite with the sea and/or pore water can alter or reset the foraminiferal geochemistry, depending on the sediment-pore water system and the sedimentary redox chemistry (McCorkle et al., 1995; Brown and Elderfield, 1996; Pena et al., 2005; Millo et al., 2005; Sexton et al., 2006; Sexton and Wilson, 2009; Edgar et al., 2013; Edgar et al., 2015; Hasenfratz et al., 2017a). While, traditional elemental proxies, such as Mg/Ca of benthic foraminifera for bottom water temperature (BWT) (e.g. Rosenthal et al., 1997; Lear et al., 2002; Elderfield et al., 2006; Lear et al., 2010), rely on the geochemistry of primary foraminiferal calcite, newly developed proxies utilise the elemental composition (i.e. U/Mn) of authigenic foraminiferal coatings that form within the sediments and could serve as a recorder of changes in the sedimentary redox environment (Gottschalk et al., 2016; Chen et al., 2017). Thus, an in-depth understanding of sedimentary diagenesis in continental margin sediments and its influence on the foraminiferal geochemistry provides an opportunity to ascertain the chemical processes involved, important for the interpretation of both primary and authigenic foraminiferal elemental proxies in these settings.

Today, vast areas of the North Pacific and the Bering Sea are considered high nutrient low chlorophyll (HNLC) regions, with iron representing the limiting micronutrient (Moore et al., 2001; Lam and Bishop, 2008). The hydrographic conditions along the eastern Bering Sea continental margin (Walsh et al., 1989; Springer et al., 1996; Mizobata et al., 2002; Mizobata and Saitoh, 2004; Mizobata et al., 2008; Expedition 323 Scientists, 2010; Hurst et al., 2010; Tanaka et al., 2012; Ladd et al., 2012), however, provide important nutrients to sustain one of the most productive ecosystems in the world's ocean, the so-called 'Green Belt' (Springer et al., 1996). Enhanced rates of primary productivity are reflected in an oxygen minimum zone (OMZ) pervasive in mid-depth waters (600–1000 m; (Whitledge and Luchin, 1999; Expedition 323 Scientists, 2010)) and sedimentary organic carbon (C_{org}) burial rates of 171–251 mmol C_{org} m^{-2} y^{-1} (Wehrmann et al., 2011), compared to <8 mmol C_{org} m^{-2} y^{-1} in typical deep sea sediments (Cartapanis et al., 2016). Thus, sub-seafloor sediments are

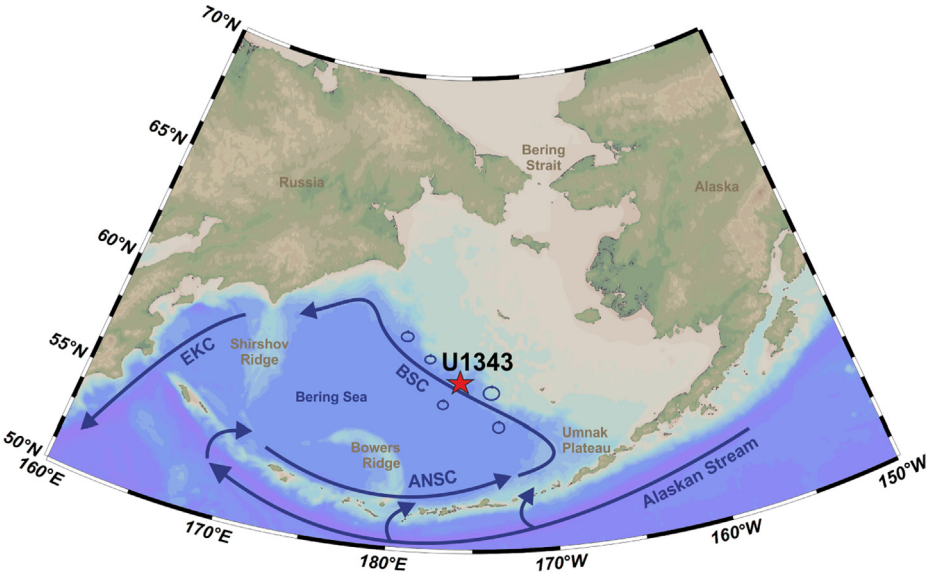

Fig. 1. Map of the Bering Sea showing the core location of IODP Site U1343 (57°33.4′N, 176°49.0′W; 1953 m water depth) (red star) and the cyclonic surface circulation (dark blue arrows). Main currents are also indicated: Aleutian North Slope Current (ANSC), Bering Slope Current (BSC) and the East Kamchatka Current (EKC). Along the eastern Bering Sea slope eddies transport nutrient rich deep waters to the surface leading to high rates of primary productivity in this region, also called the 'Green Belt' (Springer et al., 1996). (For interpretation of the references to colour in this figure legend, the reader is referred to the web version of this article.)

characterized by an active microbial community driving C_{org} remineralisation and causing the accumulation of hydrocarbons, such as methane, in deeper lying sediments (Wehrmann et al., 2011; Pierre et al., 2016).

The microbial communities driving sub-seafloor carbon cycling and C_{org} remineralisation along the eastern Bering Sea slope exploit different metabolic pathways, leading to a partitioning of reactions in the sediment column according to their metabolic efficiency (Froelich et al., 1979). Along the eastern Bering Sea slope oxic respiration occurs in the upper few centimetres of the sediment column, with an oxygen penetration depth of 10–30 cm at 1105 m and 2249 m water depth respectively (Lehmann et al., 2005). In the sub-oxic zone, nitrate (NO^{3-}) and manganese (Mn^{3+}) are reduced, followed by iron (Fe^{3+}) and sulphate (SO_4^{2-}) reduction (D'Hondt et al., 2002; Hong et al., 2013) (Eq. (1)). When all energetically more favourable terminal electron acceptors have been depleted, organic carbon is remineralised via methanogenesis (Eq. (2)) and fermentation (Berner, 1980). A distinct Sulphate-Methane Transition Zone (SMTZ) forms in sediments along the Bering Sea continental margin where the upward diffusive flux of biogenic methane meets the zone of sulphate reduction (Fig. 2) and anaerobic oxidation of methane (AOM) occurs (Eq. (3)) (Boetius et al., 2000; Wehrmann et al., 2011). Along the eastern Bering Sea slope the depth of the SMTZ varies between ~6 and 8 m below sea floor (mbsf) in response to bottom water oxygenation and the availability of labile organic matter for methanogenesis in deeper lying sediments (Wehrmann et al., 2011).

$$CH_2O + 1/2SO_4^{2-} \rightarrow 1/2H_2S + HCO_3^- \quad (1)$$

$$C_6H_{12}O_6 \rightarrow 3CH_4 + 3CO_2 \quad (2)$$

$$CH_4 + SO_4^{2-} \rightarrow HCO_3^- + HS^- + H_2O \quad (3)$$

Both organoclastic sulphate reduction and AOM form bicarbonate ions (HCO_3^-), increasing the alkalinity of ambient pore waters, facilitating authigenic carbonate formation. Calcareous foraminifera tests can act as a template for authigenic carbonate precipitation (Panieri et al., 2017; Schneider et al., 2017), altering their geochemistry. To date, most studies investigating the influence of authigenic carbonate precipitation on foraminiferal geochemistry in areas of high methane flux or even methane seepage at the seafloor have focused on the stable carbon isotopic composition ($\delta^{13}C$) (Hill et al., 2003; Hill et al., 2004; Millo et al., 2005; Martin

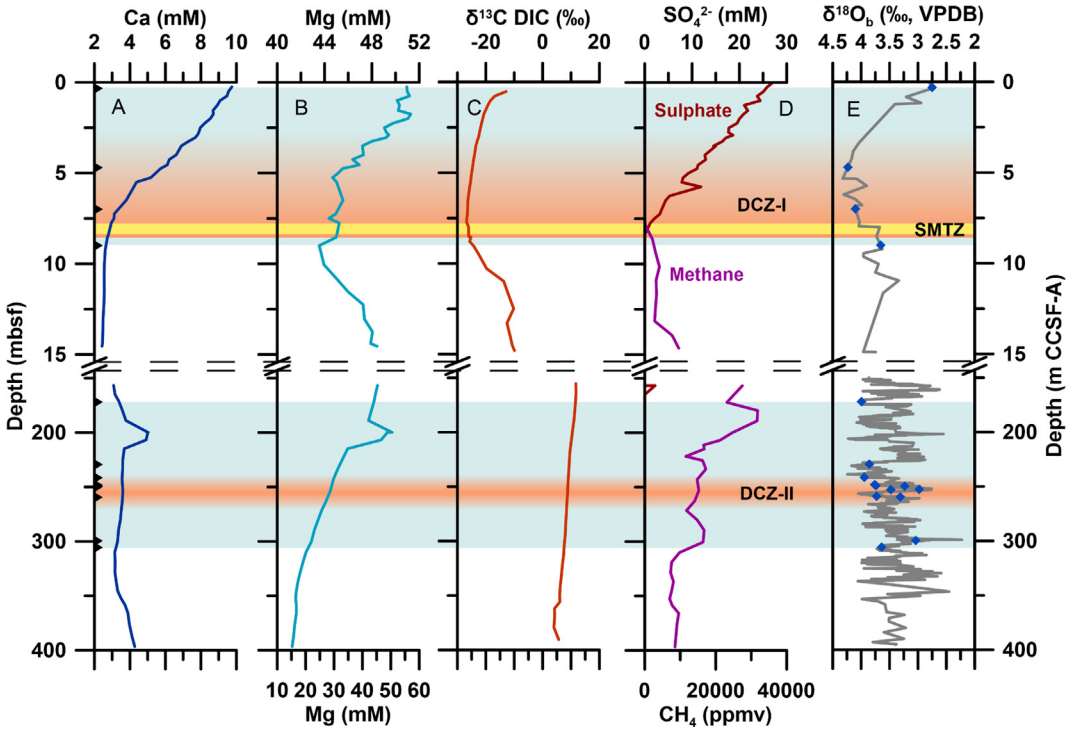

Fig. 2. Pore water profiles of (A) dissolved Ca, (B) Mg, (C) $\delta^{13}C$ of dissolved inorganic carbon (Wehrmann et al., 2011), and (D) sulphate (orange) and methane (purple) (dissolved Ca, Mg, CH_4, and SO_4^{2-} data from LIMS (hhtp://web.iodp.tamu.edu/LORE/)) at IODP Site U1343 (1953 m water depth). (E) Shows the benthic $\delta^{18}O$ record (grey) at Site U1343 across the analysed depth intervals (Asahi et al., 2016; Kender et al., 2018). Note that between 150 and 400 mbsf the $\delta^{18}O$ record represents the 5-point running mean. The dark blue diamonds (E) represent the individual samples utilized in this study, with the black triangles on the left additionally indicating the respective sample depths. The blue shaded areas mark the two depth intervals for this study, while the orange shaded areas characterize the DCZ-I and DCZ-II and the yellow horizontal bar indicates the SMTZ as seen from the sulphate and methane pore water profiles (D). Note that the axes for Mg have different scales. Pore water profiles are recorded against depth in mbsf and oxygen isotopes are recorded against depth in m CCSF-A. Dissolved pore water constituent data from LIMS (http://web.iodp.tamu.edu/LORE/). (For interpretation of the references to colour in this figure legend, the reader is referred to the web version of this article.)

et al., 2007; Cook et al., 2011; Panieri et al., 2014; Consolaro et al., 2015; Panieri et al., 2016; Panieri et al., 2017; Schneider et al., 2017; Wan et al., 2018). Compared to foraminiferal calcite, methane-related authigenic carbonates have widely varying carbon isotopic signatures, ranging from −60‰ to +26‰ (e.g. Roberts and Aharon, 1994; Hill et al., 2003; Hill et al., 2004; Naehr et al., 2007; Pierre and Fouquet, 2007; Pierre et al., 2016). In addition to the carbon isotopic signature, elevated Mg/Ca ratios have been noticed for foraminifera influenced by SMTZ-related authigenic carbonate precipitation (Panieri et al., 2017; Schneider et al., 2017; Wan et al., 2018). This is in line with authigenic carbonate crystals related to SMTZ precipitation, which are typically enriched in Mg (Aloisi et al., 2000; Aloisi et al., 2002; Crémière et al., 2012; Teichert et al., 2014). Nonetheless, a comprehensive understanding of the influence of early and late diagenetic processes on the elemental composition of foraminifera awaits the analysis of a full suite of elemental ratios.

Here we present the elemental composition (Mg/Ca, Sr/Ca, Mn/Ca, Fe/Ca, U/Ca, and Al/Ca) of shallow infaunal foraminiferal species *Elphidium batialis* Saidova (1961) at IODP Site U1343 (Fig. 1). We use a suite of single-specimen visual and geochemical evidence, including reflected light microscopy, scanning electron microscope imaging, laser ablation inductively coupled plasma mass spectrometry, and electron probe microanalysis elemental mapping, to ascertain the sedimentary diagenetic processes at play resulting in the elemental composition of both primary foraminiferal calcite and foraminiferal authigenic carbonates.

2. MATERIALS AND METHODS

2.1. Sedimentary and diagenetic setting at IODP Site U1343

Sediments at IODP Site U1343 (57°33.4′N, 176°49.0′W; 1953 m water depth) are primarily composed of dark/very dark green-grey to dark/very dark grey silt (Expedition 323 Scientists, 2010). Visually lighter and more yellow authigenic carbonate crystals can be identified in all holes at IODP Site U1343 (A–E) below ~35 mbsf (Expedition 323 Scientists, 2010). Compared to other Sites in the Bering Sea, carbonate concretions at Site U1343 are less pronounced (Expedition 323 Scientists, 2010). This likely suggests that the high rates of sediment accumulation along the eastern Bering Sea slope (21–58 cm ka^{-1}) (Expedition 323 Scientists, 2010) did not allow the SMTZ to persist at a given sediment depth long enough for distinct authigenic carbonate nodules to form (on timescales of centuries (Ussler and Paull, 2008)) (Expedition 323 Scientists, 2010). The present day SMTZ, at Site U1343, is located at ~8 mbsf, clearly seen in pore water profiles of dissolved sulphate and methane (Fig. 2) (Wehrmann et al., 2011).

Authigenic carbonate crystals occur in the form of rhombs, acicular, and globular crystals of 4–10 μm length, identified in smear slides (Expedition 323 Scientists, 2010), and are comprised of low-Mg calcite (LMC), high-Mg calcite (HMC), Fe-rich carbonates, and dolomite (Pierre et al., 2016). Based on geochemical analysis, Pierre et al. (2016) conclude that authigenic carbonates at Site U1343 form as a result of multiple diagenetic processes, including sulphate reduction, AOM, and silicate weathering. There are two distinctive formation zones, hereafter referred to as Diagenetic Carbonate Zone I (<~8 mbsf) and II (~260 mbsf) (DCZ-I, DCZ-II) (Fig. 2), reflected in the $\delta^{13}C$ signature of authigenic carbonates between +10‰ and −20‰ (Pierre et al., 2016). Early diagenetic carbonates formed in the DCZ-I are associated with low $\delta^{13}C$ values (Pierre et al., 2016), as a result of bicarbonate formation during sulphate reduction ($\delta^{13}C$: −22‰ to −26‰) and AOM ($\delta^{13}C$: −50‰ to −90‰) (Schrag et al., 2013) (Fig. 2). These are primarily composed of LMC and HMC, supported by a drawdown of dissolved Ca and Mg in the upper meters of the sediment column with a minimum in pore water concentrations at the SMTZ (Fig. 2) (Wehrmann et al., 2011; Pierre et al., 2016). On the other hand, authigenic carbonates formed in the DCZ-II, have higher $\delta^{13}C$ values (Fig. 2), characteristic of bicarbonate formed during silicate weathering within the sediments due to CO_2 formation during methanogenesis (Pierre et al., 2016). Here, Fe-rich carbonates and dolomite are more common compared to LMC and HMC in the upper diagenetic zone (Pierre et al., 2016). In addition to carbonates, other authigenic minerals in sediments along the eastern Bering Sea slope are barite and pyrite, typically precipitated during organoclastic sulphate reduction and AOM (Pierre et al., 2016).

2.2. Sampling strategy

This study focuses on two narrow depth intervals of Holocene (number of samples (n) = 4) to Pleistocene (n = 12) age between 0.33–8.99 m core composite depth below seafloor (CCSF-A) and 172.02–305.63 m CCSF-A, respectively (Fig. 2) at IODP Site U1343. An overview of the samples including the applied methodologies is given in Table 1. The two depth intervals cover the DCZ-I, comprising organoclastic sulphate reduction and AOM above and within the SMTZ, and the DCZ-II related to silicate weathering (Pierre et al., 2016), providing a comprehensive understanding of the influence of both early and late diagenetic processes on foraminiferal geochemistry. Further, the samples are derived from both glacial and interglacial intervals (Fig. 2), which likely impacts on the nature and magnitude of authigenic carbonate formation as bottom water conditions and primary productivity in the eastern Bering Sea vary on these timescales (Kim et al., 2014; Asahi et al., 2016; Kender et al., 2018).

Common infaunal benthic foraminiferal species at IODP Site U1343 include *Elphidium batialis* Saidova (1961), *Uvigerina* spp., and *Islandiella norcrossi* (Cushman, 1933). Based on the abundance and continuous occurrence, however, this study is exclusively based on *E. batialis* specimens. *E. batialis*, a shallow infaunal benthic foraminifera, forms a hyaline LMC test. In the neighbouring Sea of Okhotsk, *E. batialis* has a habitat depth in the sediment column of 0.5–1.7 cm (Bubenshchikova et al., 2008). *E. batialis* precipitates a test of medium size that is involute planispiral with nine to twelve chambers in the

Table 1
Overview of all samples used in this study, including the depth, age, size fraction, and analytical techniques for each sample.

Sample ID	Depth (m CCSF-A)	Age (ka)	Size fraction (μm)	Degree of diagenetic alteration	Methodology		
					SEM	EPMA	LA-ICP-MS
U1343C-1H-1 (32.0–34.0 cm)	0.3	8.5	>250	Minor alteration	X		X
U1343C-1H-4 (19.0–21.0 cm)	4.7	20.8	>250	Minor alteration	X		X
U1343E-1H-3 (50.0–52.0 cm)	7.0	30.1	>250	Minor alteration	X		X
U1343E-1H-4 (100.0–102.0 cm)	9.0	38.3	>250	Major alteration	X		X
U1343A-17H-5 (84.0–86.0 cm)	172.0	634.6	150–250, >250	Moderate alteration			X
U1343E-25H-2 (132.0–134.0 cm)	229.4	877.5	150–250, >250	Moderate alteration			X
U1343C-24H-7 (109.0–111.0 cm)	241.5	925.6	>250	Moderate alteration	X		X
U1343C-25H-5 (37.0–39.0 cm)	248.2	942.6	>250	Moderate alteration	X		X
U1343C-25H-5 (126.0–128.0 cm)	249.1	944.9	>250	Major alteration	X	X	X
U1343C-25H-6 (46.0–48.0 cm)	249.8	946.7	>250	Major alteration	X		X
U1343E-27H-2 W, 8.0–10.0 cm	252.6	953.9	>250	Major alteration	X		
U1343E-27H-2 W, 46.0–48.0 cm	253.0	954.9	>250	Minor alteration	X	X	
U1343C-26H-5 W, 86.0–88.0 cm	259.1	969.9	>250	Moderate alteration	X	X	
U1343C-26H-5 (126.0–128.0 cm)	259.5	970.9	>250	Minor alteration	X		X
U1343E-32H-2 (42.0–44.0 cm)	299.6	1070.1	150–250, >250	Moderate alteration			X
U1343E-32H-6 (142.0–144.0 cm)	305.6	1086.0	150–250, >250	Moderate alteration			X

final whorl (Fig. 3). The wall is finely perforate and the aperture appears as an arch of small holes. It has a rounded to lobulated outline and the chambers increase gradually in size (Fig. 3). The most distinct feature are the depressed sutures with slightly backwards curved sutural bridges (Fig. 3) (see supplement for original description). The specimens for this study were picked from the two size fractions 150–250 μm and > 250 μm. Specimens > 250 μm from Site U1343 have been previously utilized for palaeoclimate reconstructions (Asahi et al., 2016; Kender et al., 2018), however, overall benthic foraminiferal abundance is greater in the size fraction 150–250 μm.

2.3. Visual identification of foraminiferal alteration

Foraminiferal samples from IODP Site U1343 were grouped into three classes of minor, moderate, and major alteration, based on the predominant alteration state of *E. batialis* specimens using reflected light microscopy, following the approach outlined by Schneider et al. (2017). The classification includes the test colour, ranging from white to orange/brown, the translucency of the test, with increasing opaqueness indicating more alteration, and features such as a 'sugary' texture, indicating crystal growth on the outside of the foraminiferal tests, obscuring the original test structure. Little or no discolouration, translucent test walls, and prominent morphological features, such as sutural bridges for *E. batialis*, characterize minor diagenetic alteration (Fig. 4). Specimens with moderate diagenetic alteration usually have a yellow test with both translucent and opaque areas (Fig. 4), whereas discoloured orange/brown specimens with an opaque test wall, a 'sugary' texture, and obscured morphological features are classified as having major diagenetic alteration (Fig. 4).

2.4. Scanning electron microscope imaging

Scanning Electron Microscope (SEM) imaging was conducted on 12 representative *E. batialis* specimens (Table 1), exhibiting different degrees of diagenetic alteration, as determined by reflected light microscope inspection. This serves to identify the diagenetic features and microstructural changes of *E. batialis* specimens in response to carbonate diagenesis at Site U1343 and their relation to the appearances of foraminifera tests under the reflected light microscope. The samples are from above and below the SMTZ (0.3–8.9 m CCSF-A) and from around 250 ± 10 m CCSF-A. For each sample both, a whole specimen and crushed fragments were imaged. Prior to imaging all samples were ultrasonicated in UHQ water for ~10 s to remove clay minerals and other particles loosely stuck to the foraminiferal tests. Subsequently, the specimens and fragments were mounted on SEM stubs using carbon adhesive tape and gold/palladium coated. All samples were imaged on a FEI XL30 Field Emission Gun Environmental SEM at Cardiff University in high vacuum mode, with a beam voltage of 10–20 kV using a Secondary Electron Detector.

2.5. Geochemical analyses

2.5.1. Elemental analysis of foraminifera using LA-ICP-MS

Laser inductively coupled plasma mass spectrometer (LA-ICP-MS) analyses were performed at Cardiff University using an ArF excimer 193 nm laser ablation system with dual volume laser ablation cell (RESOlution S-155 ASI) coupled to a Thermo Scientific™ ELEMENT XR™ magnetic sector field ICP-MS. In total 13 samples (Table 1), were analysed with six specimens per sample and six laser spots per specimen on consecutive chambers. Based on pre-

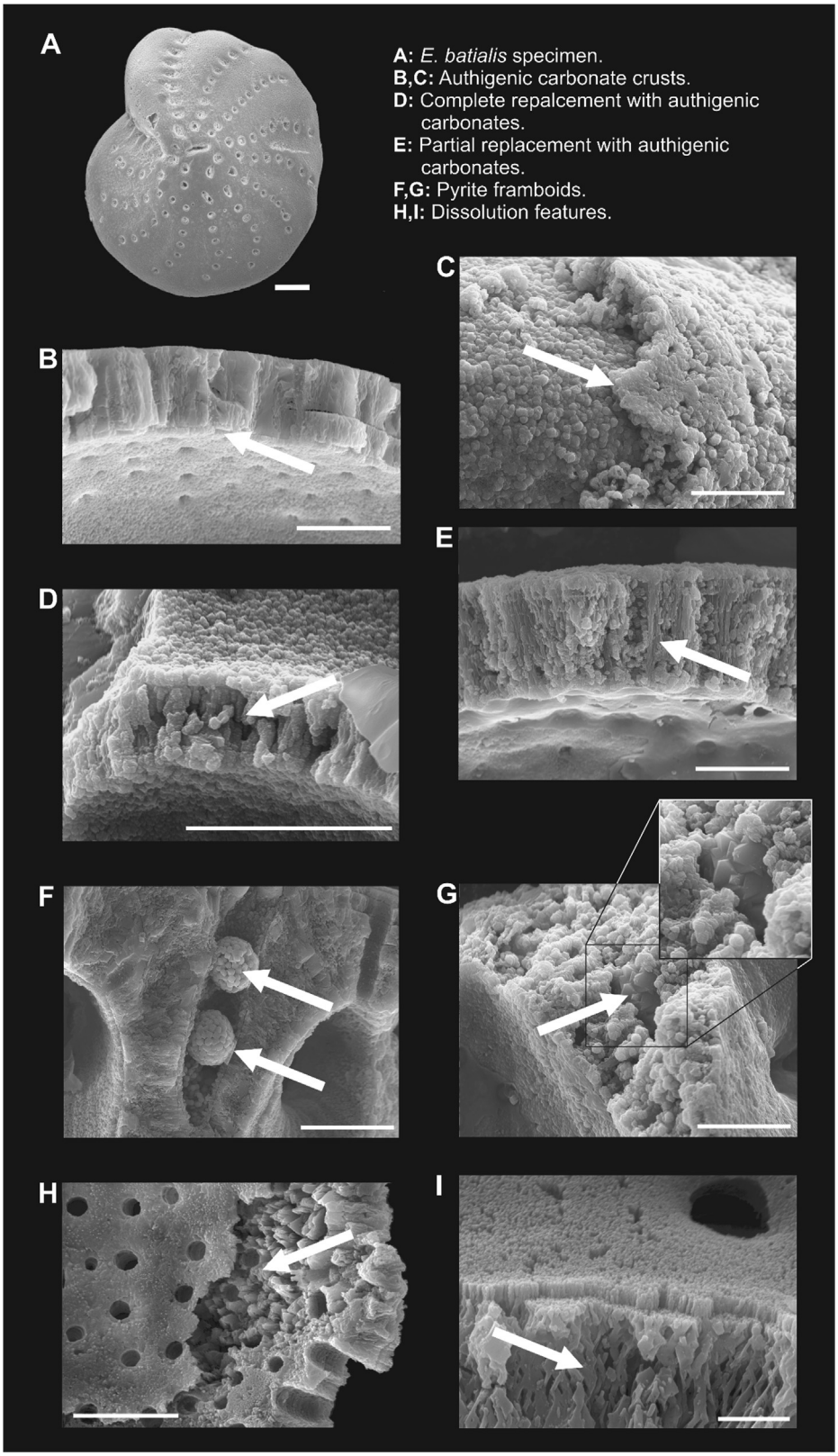
A
A: E. batialis specimen.
B,C: Authigenic carbonate crusts.
D: Complete repalcement with authigenic carbonates.
E: Partial replacement with authigenic carbonates.
F,G: Pyrite framboids.
H,I: Dissolution features.
B
C
D
E
F
G
H
I

vious investigations (Nairn, 2019) and as demonstrated in in other studies (Rathmann et al., 2004), this was found to yield statistically good results when averaging over the natural heterogeneity of foraminiferal tests. Two samples only contain two and five *E. batialis* specimens, respectively, due to low abundance. LA-ICP-MS operating conditions varied based on the size fraction of *E. batialis* specimens (Table 2) and all samples were analysed for the isotopes ^{25}Mg, ^{26}Mg, ^{27}Al, ^{43}Ca, ^{48}Ca, ^{55}Mn, ^{87}Sr, ^{88}Sr, ^{238}U. Additionally, ^{56}Fe was measured on four samples from the >250 µm size fraction, with two samples above and two samples below the DCZ-II at ~260 mbsf (Pierre et al., 2016). Because of spectral interference with ArO (May and Wiedmeyer, 1998), ^{56}Fe has to be measured in medium resolution (MR) mode of the ICP-MS, in comparison to all remaining isotopes that were measured in low resolution (LR) mode. Thus, the four samples for Fe analysis were ablated in LR mode first and re-ablated in MR mode on the same chambers. This allows direct comparison of ^{56}Fe with all other isotopes. ^{48}Ca showed spectral interference with ^{48}Ti for both glass standards NIST SRM 610 and NIST SRM 612 (see below), hampering its quantification.

The NIST SRM 612 and NIST SRM 610 silicate glass standards were used as consistency and quantification standards, respectively. NIST SRM 612 was acquired at the beginning and end of every sequence and calibrated using NIST SRM 610 for external reproducibility (Table 3). NIST SRM 612 was also used to tune the magnetic sector field ICP-MS to minimize oxide formation and elemental fractionation (ThO/Th < 0.3%, Th/U ~ 1). NIST SRM 610 was measured every six laser ablation spots and used for sample calibration. Reference values for elemental concentrations in NIST SRM 610 and 612 are from Jochum et al. (2011). Samples were calibrated using R Studio (R Studio Team, 2015) following the method outlined in Longerich et al. (1996), with ^{43}Ca as the internal standard, assuming 40 wt% for $CaCO_3$. Prior to sample calibration the limit of detection was calculated (LOD = mean gas blank + 3.3 * s.d., s.d. = standard deviation on the gas blank) for each isotope and spot and all values below the LOD were removed (Petersen et al., 2018). The high gas blank for ^{55}Mn, resulting from polyatomic interference with ^{40}Ar^{15}N (Evans and Müller, 2018), causes a relatively high LOD for ^{55}Mn measurements. Thus, ^{55}Mn could only be quantified for 22 out of 91 specimens. Additionally, signal sections classified as 'instrumental', as determined by the ^{48}Ca/^{43}Ca ratio, were removed. Sample calibration includes a gas blank and drift correction of reference materials, sample gas blank correction, and sample data reduction. Subsequently an outlier correction was performed using the Hampel identifier (Davies and Gather, 1993). Typical LA-ICP-MS profiles of foraminiferal test with minor, moderate, and major diagenetic alteration are shown in Supplementary Figs. 1–3. Lastly, the average and standard deviation was calculated of all laser profiles per specimen. ^{27}Al was used to screen for silicate contamination and most profiles show an initial peak of Al/Ca, interpreted to represent contamination on the outside of the foraminiferal test. Specimen means are integrated only for signal sections with Al/Ca below the LOD and for profiles with >10 data points of Al/Ca below the LOD, to minimize the risk of silica contribution to the sample signal. The standard deviation for single specimen means is based on the variance of the elemental ratio across the average of all laser profiles taken per specimen.

2.5.2. EPMA elemental mapping of Mg/Ca and Fe/Ca

Electron Probe Microanalysis (EPMA) elemental mapping was used to study the spatial cross-sectional distribution of Mg/Ca and Fe/Ca in three *E. batialis* specimens, representing minor, moderate, and major diagenetic alteration, respectively (Table 1). The analytical set up of the EPMA allowed only the measurement of three elements simultaneously. Mg/Ca provides an overview of authigenic carbonate distribution in the foraminiferal tests, while Fe/Ca maps offer a chance to investigate the incorporation of Fe into authigenic carbonates without potential bias due to pyrite framboids (as for LA-ICP-MS). Foraminiferal cross sections were prepared at the British Geological Survey in Keyworth, mounting the foraminiferal tests on separate glass slides and embedding them in epoxy (RT154). To expose the foraminiferal cross sections small amounts of resin were taken off at a time using a Logitech LP50 polisher with 10 µm Al-oxide powder. Subsequently the slides were polished using a sequence of 6 µm, 3 µm, 1 µm, and 0.25 µm polycrystalline diamond paste on Logitech CL50 polisher units for 30 minutes each.

The elemental maps were acquired on a JEOL 8530F field-emission EPMA equipped with 5 wavelength dispersive spectrometers at the University of Bristol. All samples and standards were silver coated, to ensure carbonate stability and to mitigate thermally driven beam damage on the sample (Smith, 1986; Kearns et al., 2014). Calcium carbonate ($CaCO_3$) was used as a standard for Ca, Diopside ($MgCaSi_2O_6$) was used for Mg, and Fe-rich Olivine ($(Mg^{2+}, Fe^{2+})_2SiO_4$) was used for Fe. Ca was measured for 10 ms on one (PETL crystal) spectrometer, whereas

Fig. 3. Scanning Electron Microscope images of one *E. batialis* specimen and wall cross sections of *E. batialis* from IODP Site U1343. (A) *E. batialis* Saidova (1961) specimen with minor diagenetic alterations from IODP Site U1343 (252.97 m CCSF-A). The scale bar (white) represents 100 µm. (B) Primary foraminiferal calcite wall with an authigenic carbonate crust on the inside of the foraminiferal test (252.97 m CCSF-A). (C) Authigenic carbonate crust on the outside of the foraminiferal test (252.59 m CCSF-A). (D) Recrystallized wall cross section with an authigenic carbonate crust (249.07 m CCSF-A). (E) Partially recrystallized test wall (252.59 m CCSF-A). (F) Pyrite framboids found in a suture of an *E. batialis* specimen. (G) Pyrite framboid inside a recrystallized test wall (252.59 m CCSF-A). (H) Etched inner surface for an *E. batialis* test (252.59 m CCSF-A). (I) Lattice-like test wall structure indicating dissolution with an authigenic carbonate crust (241.52 m CCSF-A). Scale bars for wall cross sections (white) indicate 10 µm.

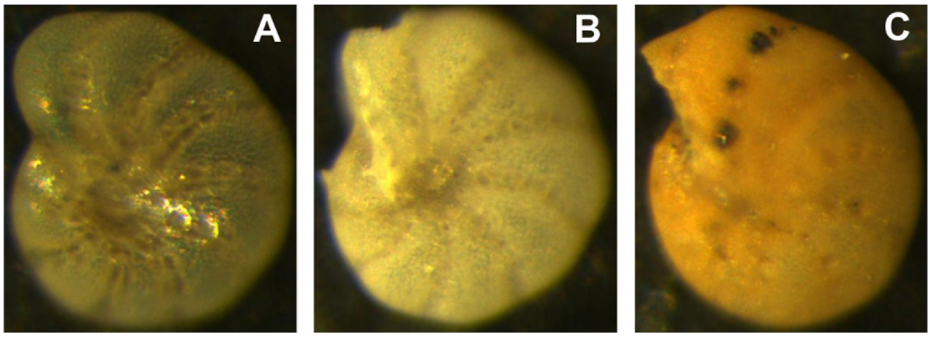

Fig. 4. Reflected light microscope images of *E. batialis* specimens with (A) minor, (B), moderate, and (C) major diagenetic alteration.

Table 2
LA-ICP-MS analytical settings for foraminiferal specimens between 150 and 250 μm, >250 μm, and the NIST 610/612 silicate glass reference standards.

	150–250 μm	>250 μm	Silicate glass reference standards NIST SRM 610 and 612
Mode	Spot analysis	Spot analysis	Raster analysis
Spot size (μm)	20	30	64
Laser fluence (J cm^{-2})	2.5	3.5	4.5
Laser pulse repetition rate (Hz)	2	4	4

Mg and Fe were measured for 300 ms each on three (two TAP crystals and one TAPH crystal) and one (LIFH/PETH crystal) spectrometers, respectively. The maps were acquired at an accelerating voltage of 15 kV, a beam current of 40 nA, and a step size of 0.5 μm. The analytical resolution, the area over which 75% of the X-rays are emitted, however, is 0.9 μm (Jonkers et al., 2016), indicating that the measured intensity for features <0.9 μm (~2 pixels) is a convolution of the actual intensity and the intensity of surrounding material. The detection limit for an average of 4 pixels is 97 ppm, 650 ppm, and 355 ppm for Mg, Ca, and Fe, respectively. Raw data were reduced to wt% according to the Armstrong/Love-Scott matrix correction (Armstrong, 1988). As the maps were acquired on predefined rectangular areas of the foraminiferal cross section, not only shell material, but also parts of the resin and other minerals were measured. Following the method outlined in Jonkers et al. (2016) Ca values under 35 wt% were masked, with the same mask applied to the Mg and Fe concentration maps, before creating the Mg/Ca and Fe/Ca maps, thus only elemental values associated with the carbonate phases are displayed in the EPMA maps. Negative Mg and Fe values were replaced with half the minimum positive value (Jonkers et al., 2016). All ratio maps were created and plotted in RStudio (R Studio Team, 2015).

2.6. Statistical analyses

Correlations of foraminiferal trace metal ratios measured by LA-ICP-MS were calculated using non-parametric bootstrapping where R^2 is based on random sampling (n = 10,000) of each elemental ratio within their respective uncertainties as represented by normal distributions. The 95% confidence intervals (CI) reported for the bootstrapped R^2 values represent bias-corrected accelerated bootstrap CIs. To test for a significant difference in the variance ($p < 0.05$) of two datasets a Wilcoxon-Mann-Whitney test or a two-sample *t*-test was performed for non-normally and normally distributed data, respectively. The Shapiro-Wilk test was used to test for normality. All statistical analyses conducted as part of this study were performed in R Studio (R Studio Team, 2015).

3. RESULTS

3.1. Foraminiferal alteration at Site U1343

Reflected light microscopy was used to group the samples into three groups of minor, moderate, and major diagenetic alterations (Fig. 4). There is a step change in the diagenetic alteration state from minor to moderate/major alteration associated with the SMTZ at the bottom of DCZ-I (Fig. 5). However, no significant change in alteration is observed at the DCZ-II (Fig. 5). Further, reflected light microscopy shows inter-sample heterogeneity within the species. The diagenetic alteration state for individual samples is thus based on the predominant alteration state of *E. batialis* specimens. Additionally, there are inter-species differences in diagenetic alteration, with *E. batialis* usually displaying stronger discolouration compared to other abundant infaunal benthic foraminiferal species at Site U1343, such as *Uvigerina* spp. and *Islandiella norcrossi*. This either indicates the importance of species-specific morphological features for post-mortem diagenetic alteration and/or different ecological preferences, which cause them to occur at times of varying organic carbon fluxes and

Table 3
Absolute elemental values and external reproducibility for the duration of this study (relative standard deviation (r.s.d.)) of NIST 612 silicate glass reference standard in LR and MR mode in comparison to absolute values from Jochum et al. (2011). ^{48}Ca concentrations in this study are influenced by spectral interference with ^{48}Ti.

	NIST SRM 612 – LR			NIST SRM 612 – MR		
Isotope	This study (ppm)	External reproducibility (r.s.d.)	Jochum et al. (2011) (ppm)	This study (ppm)	External reproducibility (r.s.d.)	Jochum et al. (2011) (ppm)
^{25}Mg	56	3.1	68 ± 5	59	8.1	68 ± 5
^{26}Mg	58	2.0	68 ± 5	58	1.7	68 ± 5
^{27}Al	12,961	1.4	10,743 ± 212	12,983	0.5	10,743 ± 211
^{43}Ca	Internal Standard		85,060 ± 715	Internal Standard		85,060 ± 715
^{48}Ca	37,148	2.3	85,060 ± 715	33,817	2.9	85,060 ± 715
^{55}Mn	39	5.2	39 ± 1	39	0.9	39 ± 1
^{57}Fe	n.a.	n.a.	51 ± 2	55	1.7	51 ± 2
^{87}Sr	51	1.7	78 ± 0.2	50	1.5	78 ± 0.2
^{88}Sr	83	3.5	78 ± 0.2	82	2.0	78 ± 0.2
^{238}U	41	4.5	37 ± 0.08	38	0.8	37 ± 0.08

microbial activity. The latter, however, requires rapid post-mortem formation of diagenetic features and subsequent mixing of different communities by bioturbation.

In support of light microscopy results, SEM imaging reveals abundant authigenic carbonates and other authigenic minerals, such as pyrite, in correlation with the degree of alteration. This is consistent with observations made during IODP Expedition 323, indicating the co-occurrence of discoloured foraminiferal tests with sedimentary authigenic carbonate crystals at Site U1343 (Expedition 323 Scientists, 2010). Authigenic carbonates can occur encrusting on the outside and/or inside of the foraminiferal tests or as partial or full recrystallization of the test walls (Fig. 3). Compared to the dense primary foraminiferal calcite layers, authigenic carbonates are characterised by stacks of tabular crystals with cavities between individual stacks (Fig. 3). Furthermore, authigenic carbonate crystals are typically larger compared to primary foraminiferal calcite, which has been previously observed in recrystallized planktonic foraminifera (Edgar et al., 2015). Both primary and authigenic calcite can be the subject of dissolution, obscuring the original features, hampering unambiguous identification (Fig. 3). Dissolution features include broken chambers, etched surfaces, and lattice-like calcite structures inside the test walls (Fig. 3). Authigenic pyrite framboids can be found inside test chambers, sutures, and even within recrystallized test walls (Fig. 3). Reflected light microscopy reveals that increased levels of pyrite typically occur in foraminiferal tests displaying a higher degree of diagenetic alteration.

3.2. LA-ICP-MS geochemical analyses

LA-ICP-MS analyses are utilised to record the elemental composition of individual *E. batialis* specimens. Table 4 documents the overall range in elemental ratios of Mg/Ca, Mn/Ca, U/Ca, Sr/Ca, and Fe/Ca.

Mg concentrations for *E. batialis* varied between 0.04 ± 0.025 wt% (s.d.) and 3.08 ± 0.39 wt% (s.d.). There is a significant increase in the Mg concentration from minor to moderate and moderate to major diagenetic alteration ($p < 0.05$) (Fig. 5), indicating that Mg is increasingly incorporated into authigenic carbonates according to the degree of diagenetic alteration. This is further supported by a significant difference in the population median ($p < 0.05$) of Mg/Ca between minor/moderate and moderate/major diagenetic alteration, respectively (Table 5).

Further, LA-ICP-MS results show that U and Sr are increased in authigenic carbonates alongside Mg. This is supported by a significant difference in the population median ($p < 0.05$) of both Sr/Ca and U/Ca between minor/-moderate and moderate/major diagenetic alteration, respectively (Table 4). In addition, both U/Ca and Sr/Ca are significantly correlated with Mg/Ca ($R^2 = 0.58$ [0.32; 0.63], n = 91 and $R^2 = 0.53$ [0.33; 0.72], n = 91, respectively) (Fig. 7).

LA-ICP-MS results also suggest Mn incorporation into authigenic carbonates, as there is a significant correlation of Mn/Ca with Mg/Ca ($R^2 = 0.64$ [0.17; 0.83], n = 21) (Fig. 7) if a single data point with anomalously high Mn/Ca (~9000 μmol mol^{-1}) is excluded. Furthermore, a significant difference in the population median ($p < 0.05$) is observed in Mn/Ca ratios of foraminifera with moderate and major diagenetic alterations (Table 5) (Fig. 6). The latter is also observed for Fe/Ca, however, there is no significant correlation with Mg/Ca (Figs. 6 and 7), likely a result of either the low numbers of Fe/Ca measurements and/or pyrite contamination.

3.3. EPMA elemental mapping of Mg/Ca and Fe/Ca

EPMA maps of *E. batialis* cross sections serve to investigate the spatial variability of Mg/Ca and Fe/Ca in tests exhibiting minor, moderate, and major diagenetic alterations (Fig. 8). SEM images of the test with minor diagenetic alterations show a thin crust of authigenic carbonates on the inside of the chamber walls, characterised by Mg/Ca ratios up to ~210 mmol mol^{-1} and Fe/Ca ratios up to ~80,000 μmol mol^{-1} as seen in the EPMA maps (Fig. 8). The moderately altered sample, on the other hand, demonstrates Mg/Ca ratios only up to ~37 mmol mol^{-1} (Fig. 8). Compared to the sample with minor alteration,

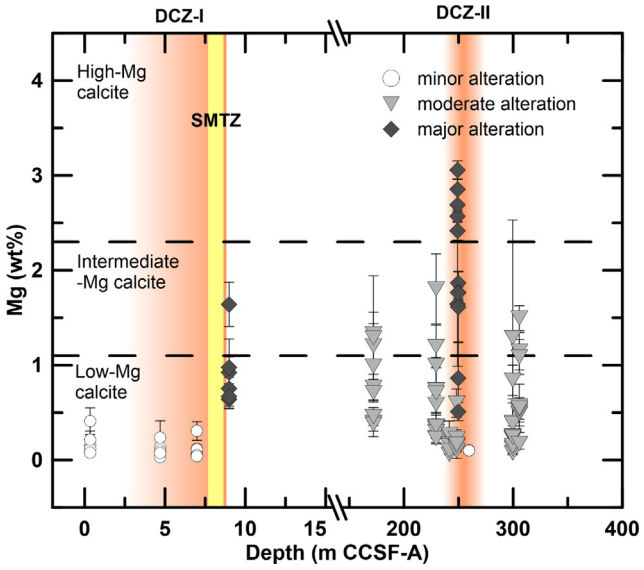

Fig. 5. Mg concentrations (wt%) in *E. batialis* specimens at IODP Site U1343 measured by LA-ICP-MS versus depth in core. The samples are coded according to the predominant diagenetic alteration state of *E. batialis* specimens: Minor diagenetic alterations (white circles), moderate diagenetic alterations (light grey triangles), major diagenetic alterations (dark grey diamonds). Error bars represent one standard deviation. The orange bars represent DCZ-I and DCZ-II and the yellow bar represents the SMTZ. Boundaries for low-Mg, intermediate-Mg, and high-Mg calcite are from Rucker and Carver (1969). (For interpretation of the references to colour in this figure legend, the reader is referred to the web version of this article.)

however, increased Mg/Ca values are found throughout the entire test wall, indicative of recrystallization (Fig. 8). This is also supported by Fe/Ca ratios, reaching up to ~65,000 μmol mol^{-1} (Fig. 8), with increased values occurring consistently throughout the test wall. SEM images of the same sample reveal isolated authigenic carbonate crystals and dissolution features within the test wall cross-section (Fig. 8). The test with major diagenetic alteration demonstrates the highest Mg/Ca and Fe/Ca ratios of up to ~270 mmol mol^{-1} and ~160,000 μmol mol^{-1}, respectively (Fig. 8). Both Mg/Ca and Fe/Ca show banding throughout the test wall cross-section co-occurring with lines of dissolution, marked by cavities within the test wall (Fig. 8). The banding is most likely related to natural laminations within the foraminiferal tests (Erez, 2003), representing lines of weakness where pore waters can enter and alter the foraminiferal calcite.

4. DISCUSSION

4.1. Multi-element composition of foraminiferal-bound authigenic carbonates at Site U1343

Morphological evidence and geochemical analyses of shallow infaunal benthic foraminiferal species *E. batialis* at IODP Site U1343 reveal visually altered tests in conjunction with prominent changes to the trace elemental composition. *E. batialis* forms a hyaline test, characterized by layered, perforate walls made of interlocking LMC microcrystals. Hence, increased Mg concentrations, observed in foraminifera from Site U1343, likely result from contamination with authigenic carbonates containing greater amounts of Mg. This is consistent with presence of the authigenic carbonate crystal assemblage found at Site U1343 composed of LMC to HMC, Fe-rich calcite, and dolomite (Pierre et al., 2016).

In order to identify the most likely authigenic carbonate mineral contaminating foraminiferal tests along the eastern Bering Sea slope, we consider the different characteristics of LMC to HMC, Fe-rich calcite, and dolomite. Dolomite usually has Mg concentrations of ~12.6 wt% (Lingling and Min, 2005), higher than the observed Mg concentrations in diagenetically altered *E. batialis* tests from Site U1343 ($<3.08 \pm 0.39$ wt% (s.d.)) (Fig. 5). If the foraminiferal tests fall along a mixing line of primary LMC and dolomite and we assume ~0.5 wt% Mg for primary foraminiferal calcite, this would require a contribution of ~20.5% dolomite in order to explain the observed Mg-concentrations. SEM images of tests with major diagenetic alteration, however, show almost complete replacement of the original foraminiferal calcite with authigenic carbonate (Fig. 3), indicating that contributions >20.5% are indeed likely. Additionally, Pierre et al. (2016) demonstrate that dolomite crystals are primarily associated with authigenic carbonate formation in the DCZ-II at ~260 mbsf. Only two samples in our study are from depth >260 mbsf and they show no significant increase in Mg concentrations and Mg/Ca ratios (Figs. 5 and 9), strongly suggesting that dolomite is unlikely to be the predominant authigenic carbonate in foraminiferal tests at IODP Site U1343.

In comparison to calcite, aragonite has a higher partition coefficient of Sr, reflected in Sr/Ca ratios around 30 mmol mol^{-1} (Bayon et al., 2007), while hyaline forami-

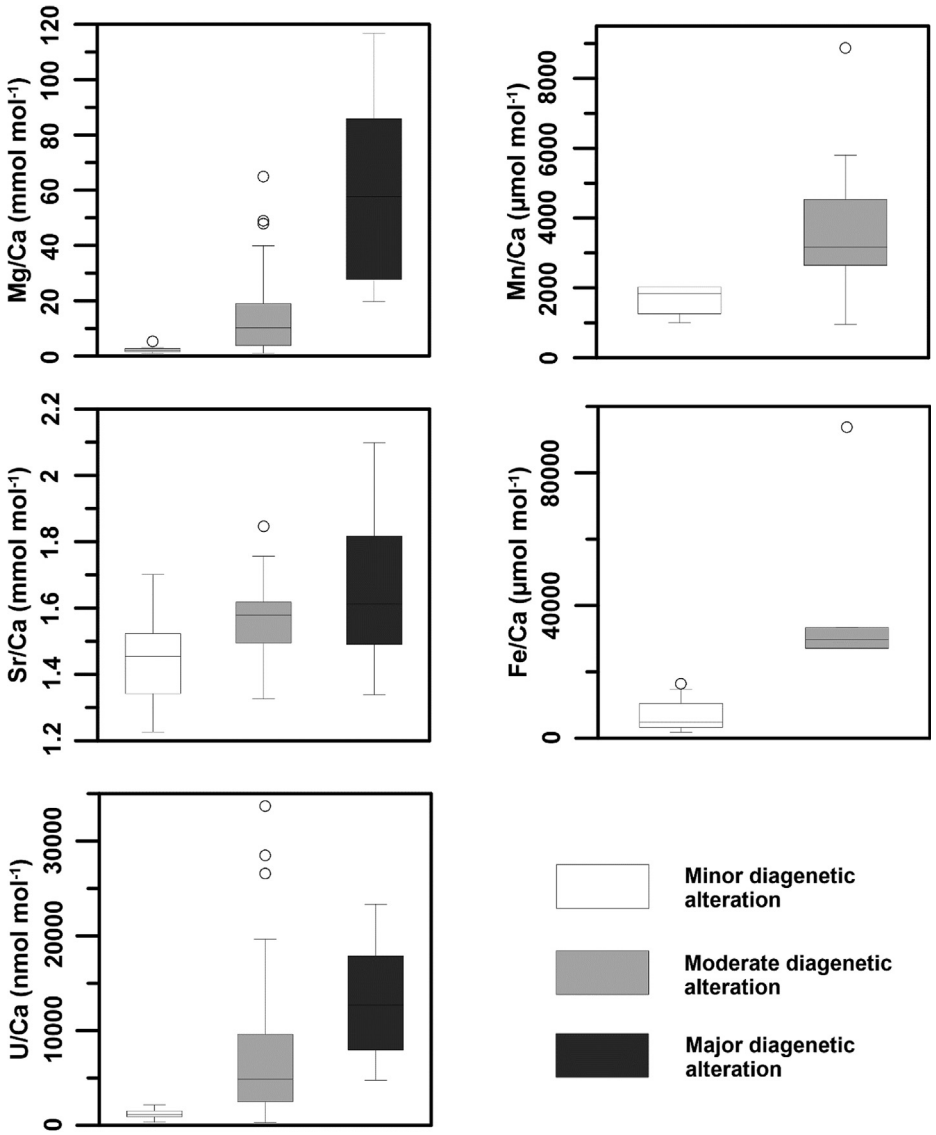

Fig. 6. Boxplots of Mg/Ca, Sr/Ca, U/Ca, Mn/Ca, and Fe/Ca (top left to bottom right) of *E. batialis* specimens measured by LA-ICP-MS and separated according to the respective degree of diagenetic alteration. The diagenetic alteration was determined using a reflected light microscope (see text) and the categories comprise minor (white), moderate (light grey), and major (dark grey) diagenetic alteration (see text).

nifera typically have Sr/Ca values of 0.75–1.25 mmol mol^{-1} (Gussone et al., 2016). Sr/Ca values of foraminiferal tests at IODP Site U1343 vary between 1.2 and 1.8 mmol mol^{-1}, with one sample (~250 m CCSF-A) showing higher Sr/Ca values between 1.8 and 2.2 mmol mol^{-1} (Fig. 9). During carbonate diagenesis aragonite is replaced with more stable carbonate species (Pierre et al., 2016). Thus, increased Sr/Ca ratios above typical values for hyaline tests are either a relic of aragonite formation during early diagenesis or related to changes in the crystal lattice due to increased Mg incorporation into authigenic carbonates. The latter is supported by a positive correlation of Mg/Ca and Sr/Ca ($R^2 = 0.53$ [0.33; 0.72], n = 91) (Fig. 7). Enhanced incorporation of Mg^{2+} results in a distortion of the calcite crystal lattice, leaving more space for the relatively large Sr^{2+} cations (Mucci and Morse, 1983). Thus, by exclusion elemental data of authigenic carbonates in foraminifera at IODP Site U1343 suggest that LMC to HMC is the most likely contaminant phase.

In addition to Sr/Ca, U/Ca is positively correlated with Mg/Ca ($R^2 = 0.58$ [0.32; 0.63], n = 91) (Fig. 7), indicating incorporation of U into authigenic calcite. Uranium in oxygenated seawater exists in form of uranyl (U^{6+}) and uranyl carbonate complexes (Klinkhammer and Palmer, 1991) with a low partition coefficient into marine calcite, as a result of its large ionic radius (Zhao et al., 2016). The largest sink for uranium in the oceans is the diffusion across the sediment-water interface and removal of soluble uranium by reduction to U^{4+} and subsequent precipitation in suboxic to anoxic environments (Klinkhammer and

Table 4
Overall range of elemental ratios for LA-ICP-MS values for samples with minor, moderate, and major diagenetic alteration including the standard deviation (s.d.).

	Minor diagenetic alteration		Moderate diagenetic alteration		Major diagenetic alteration	
Isotope ratio	Minimum ± s.d.	Maximum ± s.d.	Minimum ± s.d.	Maximum ± s.d.	Minimum ± s.d.	Maximum ± s.d.
$^{25}Mg/^{43}Ca$ (mmol mol^{-1})	1.04 ± 0.11	5.31 ± 3.34	1.08 ± 0.08	64.88 ± 31.55	19.77 ± 8.81	116.38 ± 12.88
$^{55}Mn/^{43}Ca$ (µmol mol^{-1})	n.a.	n.a.	1002.46 ± 33.71	2021.70 ± 794.05	957.97 ± 205.51	8872.33 ± 6902.53
$^{238}U/^{43}Ca$ (nmol mol^{-1})	337.29 ± 91.80	2165.83 ± 985.90	281.91 ± 33.10	33678.40 ± 10636.70	4764.42 ± 1799.09	23348.10 ± 2138.48
$^{88}Sr/^{43}Ca$ (µmol mol^{-1})	1.23 ± 0.04	1.88 ± 0.92	1.33 ± 0.02	1.85 ± 0.23	1.34 ± 0.04	2.10 ± 0.13
$^{56}Fe/^{43}Ca$ (µmol mol^{-1})	n.a.	n.a.	1808.34 ± 396.40	16404.49 ± 7485.87	27091.38 ± 5938.64	93709.67 ± 170415.71

Palmer, 1991; Zhao et al., 2016). As the ionic radius of U^{4+} is similar to that of Ca^{2+} cations, U^{4+} can be readily incorporated into carbonates forming within the sediment (Sturchio et al., 1998; Zhao et al., 2016). Typical U/Ca values of primary foraminiferal calcite range from 3-23 nmol mol^{-1} (Russell et al., 2004; Raitzsch et al., 2011; Boiteau et al., 2012; Chen et al., 2017). Foraminiferal U/Ca ratios at Site U1343 vary between 299 ± 111 nmol mol^{-1} to 29,098 ± 13,826 nmol mol^{-1} (s.d.), supporting U incorporation in authigenic carbonates during foraminiferal diagenesis.

Similar to U, Mn/Ca and Mg/Ca are significantly correlated if one data point with anomalously high Mn/Ca is excluded ($R^2 = 0.64$ [0.17; 0.83], n = 21) (Fig. 7). As suggested in previous studies, this indicates Mn^{2+} incorporation into authigenic carbonates formed within the sediments (Pena et al., 2005; Torres et al., 2010; Groeneveld and Filipsson, 2013; Hasenfratz et al., 2017a). In addition to authigenic carbonate phases Mn can also be incorporated into Mn-Fe-oxides coatings on foraminiferal tests (Pena et al., 2005; Pena et al., 2008). Mn-Fe-oxides form within the sediments above the oxygen penetration depth and Mn can be re-mobilized and dissolved into pore waters as Mn^{2+} under reducing conditions (Froelich et al., 1979). If all the foraminiferal Mn contamination at IODP Site U1343 was derived from Mn-Fe-oxides, a Mg/Mn ratio close to that of global Mn-Fe-oxide crusts/nodules of 0.2 mol mol^{-1} (de Lange et al., 1992; Pattan, 1993) would be expected. However, all specimens have a Mg/Mn ratio higher (2.47–26.10 mol mol^{-1}) than that of global Mn-Fe-oxide crusts/nodules (2.47–26.10 mol mol^{-1}). This suggests that Mn-Fe-oxides are not the predominant contaminant phase in foraminifera along the eastern Bering Sea slope, even though the possibility of Mn-Fe-oxide contribution cannot be fully eliminated. In particular, high Mn/Ca ratios (~8500 µmol mol^{-1}) at low Mg/Ca in one specimen, in conjunction with relatively high Fe/Ca of ~35,000 µmol mol^{-1} (Fig. 7), could result from contribution of Mn-Fe-oxides. Previous studies have suggested that Fe-Mn-oxides crusts on foraminiferal tests get covered by authigenic carbonates deeper in the sediment column, hampering the dissolution and resumption of Mn into pore waters under reducing conditions (Pena et al., 2005).

Fe/Ca values were measured in 4 samples (20 specimens), primarily to test the influence of authigenic Fe-rich carbonate and dolomite formation in the DCZ-II (~260 mbsf (Pierre et al., 2016)) on foraminifera at IODP Site U1343. LA-ICP-MS results show no significant correlation of Fe/Ca with Mg/Ca and no significant change across the DCZ-II (Figs. 7 and 9). However, Fe-Mn-oxide and especially pyrite (FeS_2) contamination in foraminiferal tests could bias LA-ICP-MS analyses of Fe/Ca. Fe/Ca ratios of EPMA maps, on the other hand, cannot be associated with pyrite or Mn-Fe-oxides, as areas with Ca concentrations <35 wt% have been masked in order to display the carbonate phases only. Fe/Ca values in EPMA maps of foraminiferal cross sections are elevated in areas displaying increased Mg/Ca ratios (Fig. 8), suggesting that Fe, alongside Mg, Sr, U, and Mn is incorporated into the authigenic carbonates.

Our geochemical analyses of *E. batialis* specimens at IODP Site U1343 therefore demonstrate abundant LMC to HMC contamination, in line with increased Mg concentrations in methane-related foraminiferal authigenic carbonates from the western Svalbard margin (Panieri et al., 2017; Schneider et al., 2017). In addition to Mg, authigenic carbonates at IODP Site U1343 are enriched in Sr, U, Mn, and Fe compared to the primary foraminiferal calcite, indicating important implications for palaeoenvironmental reconstructions based on these elements.

4.2. The origin of foraminiferal-bound authigenic calcite within the sediment-pore water system

Across the SMTZ there is a significant increase in Mg/Ca and U/Ca ($p < 0.05$), observed in single specimen LA-ICP-MS measurements (Fig. 9). Additionally, Mn/Ca ratios of *E. batialis* are above the LOD just below the present day SMTZ, in contrast to samples from above the SMTZ (Fig. 9), suggesting that foraminiferal Mn/Ca also increases across this redox horizon. The increase in diagenetic alteration across the SMTZ is supported by reflected light microscope results, indicating minor foraminiferal alterations above the SMTZ and moderate/major alterations below (Table 1). Thus, foraminiferal tests are significantly altered during early diagenesis across the SMTZ, where AOM causes the formation of bicarbonate ions, increasing the alkalinity of pore waters and causing the precipitation of authigenic calcite. This is consistent with previous studies of benthic foraminiferal diagenesis in areas influenced by methane seeps (Millo et al., 2005; Martin et al., 2007; Cook et al., 2011; Panieri et al., 2014; Consolaro et al., 2015; Panieri et al., 2016; Panieri et al., 2017; Schneider et al., 2017), suggesting high-Mg authigenic carbonate formation within the SMTZ (Panieri et al., 2017; Schneider et al., 2017). Additionally, Mg and Ca pore water profiles at Site U1343 decrease towards the SMTZ, indicating precipitation of Mg-calcite (Fig. 2) (Wehrmann et al., 2011).

SEM images of three foraminiferal specimens from samples above the present day SMTZ show primarily dissolution of the original calcite tests, but also provide some evidence for authigenic carbonate precipitation (Fig. 10). There are two possible mechanisms that could cause the presence of authigenic carbonates above the present day SMTZ: (1) past migration of the SMTZ in relation to changes in the sedimentary redox chemistry and (2) authigenic carbonate precipitation as a result of organoclastic sulphate reduction. LA-ICP-MS results demonstrate significant differences in the chemical composition of authigenic carbonates above and below the present day SMTZ (Fig. 9), characterised by a significant increase in Mg/Ca and U/Ca ratios (Fig. 9). Dissolved sulphate in pore waters above the SMTZ effectively complexes Mg^{2+} cations (Walter, 1986), making it unavailable for incorporation into authigenic carbonates. The significantly lower Mg/Ca ratios of foraminifera above the SMTZ (Fig. 9), thus suggest authigenic carbonate precipitation in response to bicarbonate formation (Eq. (1)) during organoclastic sulphate reduction rather than migration of the SMTZ.

Previous studies of methane-related carbonate pavements on the seafloor suggest aragonite precipitation in sulphate-rich environments (Aloisi et al., 2002; Bayon et al., 2009). There is no significant difference in the Sr/Ca ratios of *E. batialis* specimens above and below the SMTZ at Site U1343 (Fig. 9), contradicting aragonite formation in the zone of organoclastic sulphate reduction. Hence, geochemical evidence suggests that LMC formation may be favoured above the present day SMTZ at IODP Site U1343, while intermediate Mg-calcite (IMC) to HMC precipitation occurs within the SMTZ.

Reflected light microscopy and SEM images of foraminifera from both above and below the SMTZ at Site U1343 demonstrate the presence of pyrite framboids within the foraminiferal tests (Figs. 3 and 10). Abundant pyrite formation within the sediments typically occurs in the zone of organoclastic sulphate reduction, producing H_2S (Berner, 1984; Peckmann et al., 2001; Lin et al., 2016), and in the SMTZ, where AOM leads to the formation of HS^- (Lin et al., 2016). Notably, some foraminifera even show pyrite framboids within recrystallized test walls (Fig. 3), suggesting co-precipitation of authigenic carbonates and pyrite framboids, supporting a primarily early diagenetic origin of foraminiferal-bound authigenic carbonates.

Across the DCZ-II (~260 mbsf), as proposed by Pierre et al. (2016), there is no significant change in the foraminiferal geochemistry (Fig. 9). This strongly suggests that early diagenetic alterations linked to organoclastic sulphate reduction and AOM are the primary causes of changes in foraminiferal geochemistry in methane-bearing continental margin sediments.

4.3. Palaeoceanographic implications

The Mg/Ca of benthic foraminifera is a widely applied and accepted proxy in palaeoceanography to reconstruct changes in BWT through time (e.g. Rosenthal et al., 1997; Martin et al., 2002; Lear et al., 2002). In conjunction with benthic foraminiferal oxygen isotopes this allows determination of the seawater oxygen isotope composition, a proxy

Table 5
Statistical results of Mann-Whitney and 2 sample *t*-tests for elemental ratios according to their degree of diagenetic alteration.

	p-Value for minor/moderate	p-value for moderate/major	Statistical analysis
Mg/Ca	4.56E−08	7.37E−08	Mann-Whitney test
Sr/Ca	0.02	0.03	2 sample *t*-test
U/Ca	3.03E−09	6.100E−05	Mann-Whitney test
Fe/Ca	n.a.	0.0002	Mann-Whitney test
Mn/Ca	n.a.	0.02	Mann-Whitney test

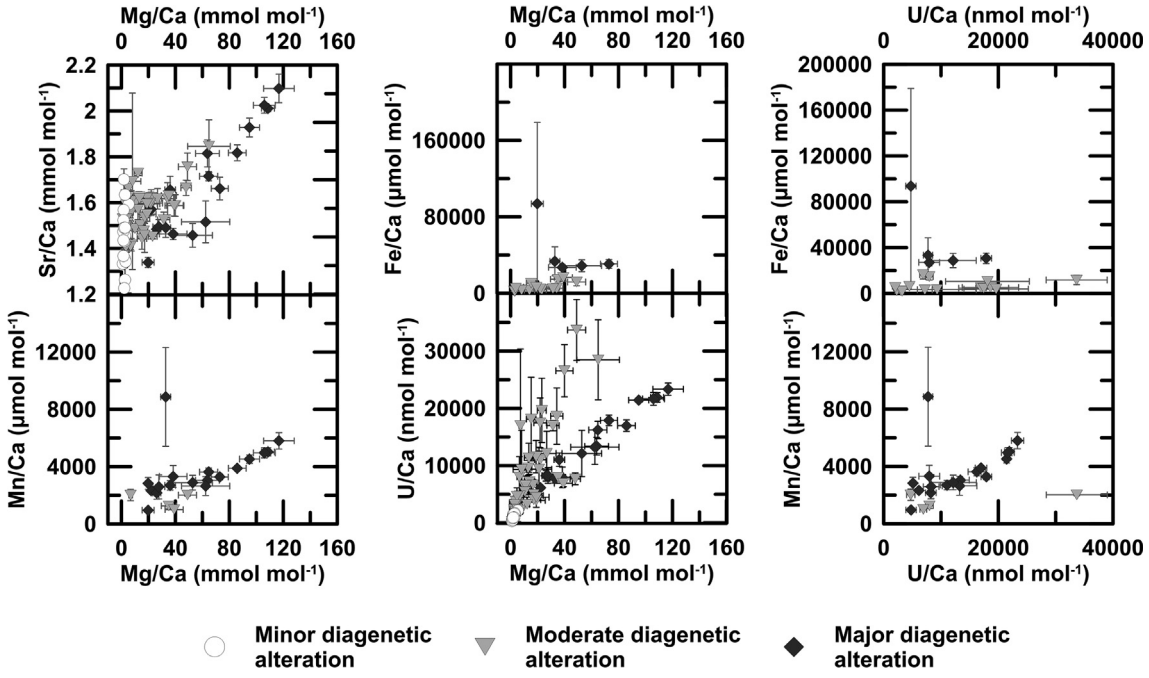

Fig. 7. Correlations of various mean single specimen LA-ICP-MS foraminiferal trace metal ratios. Error bars represent one standard deviation. The samples are coded according to the predominant diagenetic alteration state of *E. batialis* specimens: Minor diagenetic alterations (white circles), moderate diagenetic alterations (light grey triangles), major diagenetic alterations (dark grey diamonds).

for continental ice volume important to understand climate sensitivity in the past. Such climate reconstructions rely on the geochemical integrity of foraminiferal tests. Common hyaline LMC benthic foraminiferal species in the arctic to subarctic realm, such as *Cassidulina neoteretris*, *Nonionella labradorica*, *Elphidium clavatum*, *Uvigerina* spp., and *Melonis barleeanum* have Mg/Ca ratios ranging from ~0.5 to 1.5 mmol mol^{-1} (Lear et al., 2002; Elderfield et al., 2006; Kristjánsdóttir et al., 2007; Skirbekk et al., 2016; Hasenfratz et al., 2017b; Barrientos et al., 2018). At IODP Site U1343 *E. batialis* LA-ICP-MS Mg/Ca ratios vary from ~1 to 116 mmol mol^{-1} (Fig. 7), as a result of authigenic calcite contamination, yielding highly unrealistic BWT values if a similar Mg/Ca BWT sensitivity as *E. clavatum* is assumed (Mg/Ca = 0.816 ± 0.06 + 0.125 ± 0.05 * BWT) (Barrientos et al., 2018).

Typically, studies of foraminiferal Mg/Ca include rigorous chemical cleaning procedures, including a clay removal step, oxidative treatment to remove remnant organic matter, reductive treatment to remove Mn-Fe-oxides, and a weak acid leach to remove adsorbed contaminants on the foraminiferal fragments (Boyle, 1983; Barker et al., 2003). Although some authigenic carbonate contamination may be removed during reductive cleaning (Pena et al., 2005), methane-related authigenic carbonates have been shown to be tightly intergrown with primary foraminiferal calcite (Panieri et al., 2017; Schneider et al., 2017) making their removal more difficult. Furthermore, Yu et al. (2007) showed that the reductive step can cause partial dissolution of the primary foraminiferal calcite reducing the primary foraminiferal Mg/Ca ratio. It is therefore crucial to determine the composition and nature of authigenic foraminiferal contamination phases prior to palaeoenvironmental reconstructions and to conduct a detailed cleaning study in order to adjust the methodology accordingly.

EPMA analyses of *E. batialis* specimens from Site U1343 reveal the spatial variability of authigenic carbonates within the foraminiferal test walls. Tests with moderate/major diagenetic alteration are characterised by increased Mg/Ca values throughout the test wall. This can be either due to recrystallization or result from dissolution of the primary calcite and precipitation of authigenic IMC to HMC along natural laminations within the test walls (Fig. 8). Tests with minor diagenetic alteration on the other hand show a thin authigenic carbonate crust on the inside of the test wall (Fig. 8). Paleoenvironmental reconstructions based on foraminifera with minor diagenetic alteration are possible if the authigenic carbonate crust can be accounted for or removed during chemical cleaning (i.e. reductive treatment (Boyle, 1983)). Another approach would be to use LA-ICP-MS single specimen analyses to distinguish between primary foraminiferal and authigenic calcite. Trace metal ratios of foraminifera with moderate and major alterations on the other hand, need to be treated with additional caution (e.g. detailed visual and chemical single-specimen analyses and screening for contaminants during analysis), to ensure that the resulting proxy reconstructions are meaningful.

Previous approaches to mathematically account for authigenic Mg contribution include regression of Mg/Ca and a trace metal primarily associated with the contamination phase (Lea et al., 2005) or determination of the Mg/metal ratios in the contaminant (Hasenfratz et al., 2017a). Both methods, however, assume a constant Mg/metal ratio

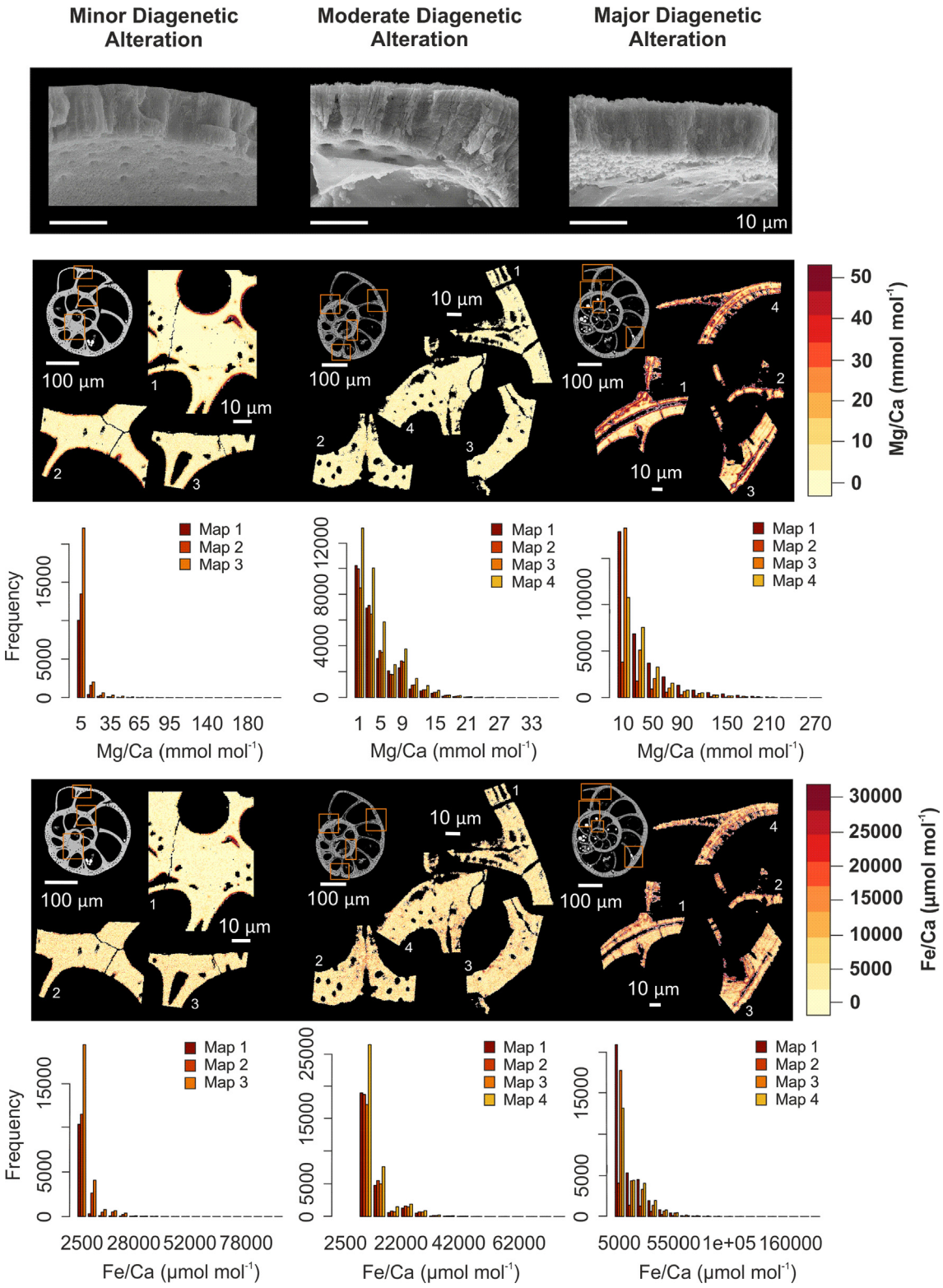

Fig. 8. SEM images of foraminiferal wall cross sections and EPMA maps of Mg/Ca and Fe/Ca of the same samples for three specimens of *E. batialis* representative of minor, moderate, and major diagenetic alteration (Table 1). Mg/Ca and Fe/Ca maps have been capped at 50 mmol mol^{-1} and 30,000 µmol mol^{-1}, respectively, to ensure good visual representation of the authigenic carbonate phases. Histograms below the maps, however, demonstrate the full range of elemental ratios.

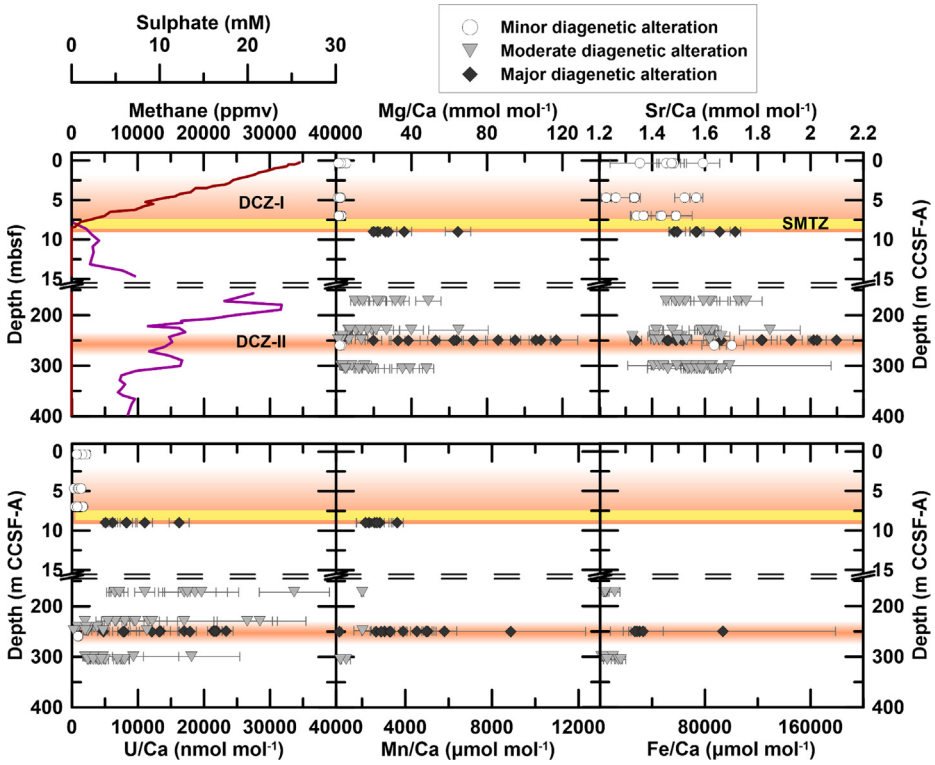

Fig. 9. Sulphate (dark red) and methane (purple) pore water profiles at IODP Site U1343 together with LA-ICP-MS Mg/Ca, Sr/Ca, U/Ca, Mn/Ca, and Fe/Ca ratios of *E. batialis* versus depth. The samples are coded according to the predominant diagenetic alteration state of *E. batialis* specimens: Minor diagenetic alterations (white circles), moderate diagenetic alterations (light grey triangles), major diagenetic alterations (dark grey diamonds). Error bars represent one standard deviation. The orange horizontal bars represent the DCZ-I and DCZ-II and the yellow horizontal bars shows the depth of the SMTZ. Pore water profiles are recorded against depth in mbsf while LA-ICP-MS results are recorded against depth in m CCSF-A. Dissolved pore water constituent data from LIMS (http://web.iodp.tamu.edu/LORE/). (For interpretation of the references to colour in this figure legend, the reader is referred to the web version of this article.)

in the contamination phase (Lea et al., 2005; Hasenfratz et al., 2017a). At Site U1343, Mg/metal ratios, such as Mg/Mn or Mg/U are highly variable, likely because of changes to the sedimentary redox-chemistry, affecting the distribution coefficients of trace metals between the solid and the liquid phase. This highlights that further research is needed to fully understand the mechanisms controlling Mg, U, and Mn incorporation into authigenic carbonates in methane-bearing sediments, before a mathematical correction of foraminiferal Mg/Ca ratios becomes possible at these sites.

We thus propose to conduct detailed cleaning studies using an element primarily associated with the authigenic calcite to screen for contamination. Geochemical results of *E. batialis* at Site U1343 suggest that U/Ca is a valuable tracer to determine methane-related authigenic carbonate contamination in continental margin settings. Typical U/Ca ratios of primary foraminiferal calcite are very small compared to measured U/Ca ratios at Site U1343, suggesting disproportionately enhanced uranium incorporation into authigenic carbonates. Furthermore, U/Ca ratios are increased in both LMC and IMC to HMC authigenic carbonates formed above and within the SMTZ. The U/Ca ratios are also unlikely to be influenced by additional authigenic minerals, such as Mn-Fe-oxides and pyrite, identifying U/Ca as a universal tracer of authigenic carbonate contamination across varying redox regimes. A U/Ca threshold for authigenic carbonate contamination, however, is likely to vary between investigations, depending on the study site and the chemical cleaning procedures applied.

In addition to primary foraminiferal trace metal ratios, recent studies suggest authigenic foraminiferal U/Mn as a proxy for sedimentary redox conditions (e.g. Gottschalk et al., 2016; Chen et al., 2017). At IODP Site U1343 an increase in U/Ca and Mn/Ca ratios can be observed in foraminifera with a higher degree of diagenetic alteration (Fig. 11). Even though both U/Ca and Mn/Ca correlate with the degree of diagenetic alteration, the increase in U/Ca is proportionally larger (Fig. 11), possibly reflecting more reducing conditions in the sediments and changes in the sedimentary redox chemistry through time. However, the large increase in U/Ca and Mn/Ca associated with the SMTZ (Fig. 9) could also reflect concentration of these elements within this redox horizon, potentially complicating the use of authigenic foraminiferal trace metals as proxy indicators, at least for samples from below the SMTZ, highlighting the need for additional research in this area.

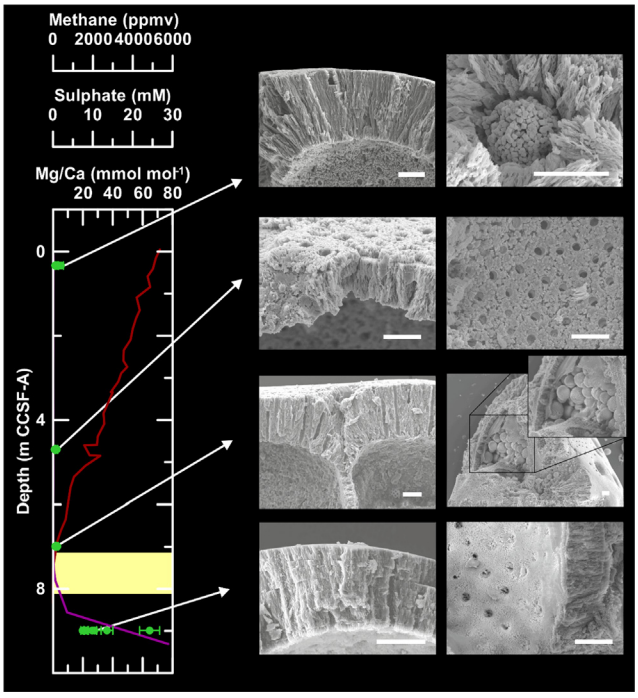

Fig. 10. Scanning Electron Microscope images of *E. batialis* specimens across the upper 9 m CCSF-A, spanning the present day SMTZ (yellow bar) (Wehrmann et al., 2011) together with the sulphate (dark red) and methane (purple) pore water profiles and the Mg/Ca ratios. Scale bars (white) represent 10 μm. (For interpretation of the references to colour in this figure legend, the reader is referred to the web version of this article.)

5. CONCLUSIONS

Visual and geochemical evidence of the benthic foraminiferal species *E. batialis* at IODP Site U1343, underlying the high productivity region of the 'Green Belt' in the eastern Bering Sea, demonstrates the presence of authigenic calcite and authigenic pyrite framboids. Foraminiferal authigenic calcite is of early diagenetic origin and forms within the zones of organoclastic sulphate reduction and AOM above and within the SMTZ, respectively. Authigenic calcite formed within the SMTZ is characterised by a higher Mg concentration compared to authigenic calcite formed above this redox horizon, likely as a result of the inhibiting effect of pore water sulphate concentrations on Mg incorporation into inorganically precipitated carbonates.

In addition to increased Mg concentrations, authigenic calcite is characterised by increased U/Ca, Mn/Ca, Fe/Ca, and Sr/Ca ratios compared to primary foraminiferal calcite. While the incorporation of U, Mn, and Fe into authigenic carbonates is likely controlled by the sedimentary redox chemistry, indicating precipitation under suboxic conditions, increased Sr/Ca ratios most likely result from distortion of the calcite crystal lattice caused by higher Mg concentrations.

EPMA maps of Mg/Ca and Fe/Ca in foraminiferal cross sections reveal the spatial distribution of authigenic calcite and other diagenetic features in foraminifera with different degrees of diagenetic alterations. The observed features include, authigenic calcite crusts, dissolution and recrystallization of primary foraminiferal calcite, and authigenic calcite banding along biologically defined laminations within the test wall. Detailed cleaning studies and contamination thresholds need to be applied when using foraminifera from methane-bearing continental margin sediment in paleoenvironmental reconstructions. Alternatively, foraminiferal

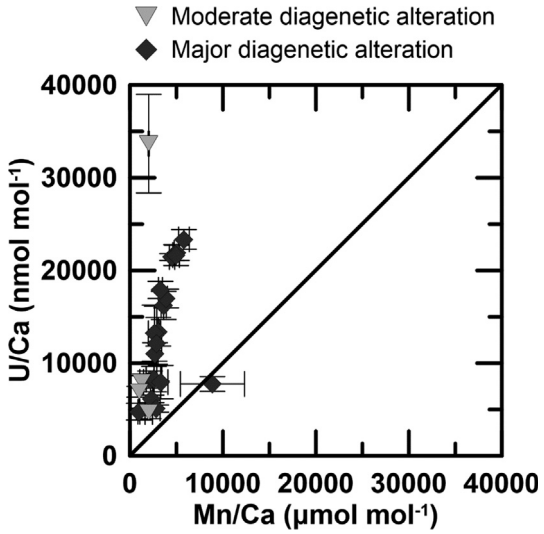

Fig. 11. U/Ca versus Mn/Ca of mean single specimen LA-ICP-MS analyses of *E. batialis* at IODP Site U1343. The samples are coded according to the predominant diagenetic alteration state of *E. batialis* specimens as determined from reflected light microscopy: Moderate diagenetic alterations (light grey triangles) and major diagenetic alterations (dark grey diamonds).

trace metals can be measured by LA-ICP-MS, able to distinguish between primary foraminiferal and authigenic calcite.

At Site U1343 U/Ca ratios appear to be a promising tracer of authigenic carbonate contamination. Uranium incorporation into authigenic carbonates is disproportionately enhanced compared to primary foraminiferal calcite and is observed in carbonates formed during organoclastic sulphate reduction and AOM. Furthermore, U/Ca ratios are only marginally influenced by additional authigenic mineral phases, such as Mn-Fe-oxides and pyrite, altering the authigenic Mn/Ca and Fe/Ca values. The individual U/Ca thresholds however are likely to vary between studies based on the study location and the analytical procedures.

On the other hand, authigenic carbonates also offer exciting new opportunities to study sedimentary redox chemistry through time. Both U/Ca and Mn/Ca ratios of foraminifera at IODP Site U1343 increase with a higher degree of diagenetic alteration, while the increase in U/Ca is proportionally larger compared to Mn/Ca possibly reflecting changes of sedimentary redox chemistry through time. However, further research is needed regarding the influence of SMTZ processes on redox sensitive trace metals, to ultimately determine the mechanisms responsible for trace metal incorporation into authigenic carbonates formed within this redox horizon.

Thus, although authigenic carbonates complicate the applicability of established palaeoclimate proxies such as Mg/Ca for BWT, after careful visual and geochemical investigation, including a cleaning test, this study demonstrates that foraminifera from methane-bearing continental margin sediments can still be utilised for palaeoenvironmental reconstructions. Additional research is necessary to fully elucidate the mechanisms controlling trace metal incorporation into authigenic carbonates. This will aid to account for authigenic carbonate contamination in climate reconstructions, but also provide information with respect to microbial processes and sedimentary redox chemistry, linked to primary productivity and bottom water oxygenation, important players in the marine carbon cycle.

ACKNOWLEDGEMENTS

H.D. would like to acknowledge funding through a Natural Environmental Research Council (NERC) Ph.D. research grant (NE/L002434/1), via the GW4+ Doctoral Training Partnership and additional funding provided by a BGS University Funding Initiative Ph.D. studentship (S268). Thank you to Katrine Husum for very helpful comments on the first version of this manuscript and for providing parts of the sample material. Thank you to Michael Nairn for helping with the LA-ICP-MS analyses and thank you to James McManus for helpful discussion of authigenic uranium cycling in continental margin sediments. Marine sediment samples were provided as part of the International Ocean Discovery Program.

APPENDIX A. SUPPLEMENTARY MATERIAL

Supplementary data to this article can be found online at https://doi.org/10.1016/j.gca.2019.09.025.

REFERENCES

Aloisi G., Bouloubassi I., Heijs S. K., Pancost R. D., Pierre C., Damsté J. S., Gottschal J. C., Forney L. J. and Rouchy J. M. (2002) CH4-consuming microorganisms and the formation of carbonate crusts at cold seeps. *Earth Planet. Sci. Lett.* **203**, 195–203.

Aloisi G., Pierre C., Rouchy J.-M., Foucher J.-P. and Woodside J. (2000) Methane-related authigenic carbonates of eastern Mediterranean Sea mud volcanoes and their possible relation to gas hydrate destabilisation. *Earth Planet. Sci. Lett.* **184**, 321–338.

Armstrong J. (1988) Quantitative analysis of silicate and oxide materials: comparison of Monte Carlo, ZAF and $\phi(\rho z)$ procedures. San Francisco Press, San Francisco.

Asahi H., Kender S., Ikehara M., Sakamoto T., Takahashi K., Ravelo A. C., Alvarez Zarikian C. A., Khim B. K. and Leng M. J. (2016) Orbital-scale benthic foraminiferal oxygen isotope stratigraphy at the northern Bering Sea Slope Site U1343 (IODP Expedition 323) and its Pleistocene paleoceanographic significance. *Deep Sea Res. Part II Top. Stud. Oceanogr.* **125–126**, 66–83.

Barker S., Greaves M. and Elderfield H. (2003) A study of cleaning procedures used for foraminiferal Mg/Ca paleothermometry. *Geochem. Geophys. Geosyst.* **4**, 8407.

Barrientos N., Lear C. H., Jakobsson M., Stranne C., O'Regan M., Cronin T. M., Gukov A. Y. and Coxall H. K. (2018) Arctic Ocean benthic foraminifera Mg/Ca ratios and global Mg/Ca-temperature calibrations: new constraints at low temperatures. *Geochim. Cosmochim. Acta* **236**, 240–259.

Bayon G., Loncke L., Dupré S., Caprais J.-C., Ducassou E., Duperron S., Etoubleau J., Foucher J.-P., Fouquet Y., Gontharet S., Henderson G. M., Huguen C., Klaucke I., Mascle J., Migeon S., Olu-Le Roy K., Ondréas H., Pierre C., Sibuet M., Stadnitskaia A. and Woodside J. (2009) Multi-disciplinary investigation of fluid seepage on an unstable margin: the case of the Central Nile deep sea fan. *Mar. Geol.* **261**, 92–104.

Bayon G., Pierre C., Etoubleau J., Voisset M., Cauquil E., Marsset T., Sultan N., Le Drezen E. and Fouquet Y. (2007) Sr/Ca and Mg/Ca ratios in Niger Delta sediments: implications for authigenic carbonate genesis in cold seep environments. *Mar. Geol.* **241**, 93–109.

Berner R. A. (1980) Early Diagenesis: A Theoretical Approach. Princeton University Press.

Berner R. A. (1984) Sedimentary pyrite formation: an update. *Geochim. Cosmochim. Acta* **48**, 605–615.

Boetius A., Ravenschlag K., Schubert C. J., Rickert D., Widdel F., Gieseke A., Amann R., Jørgensen B. B., Witte U. and Pfannkuche O. (2000) A marine microbial consortium apparently mediating anaerobic oxidation of methane. *Nature* **407**, 623–626.

Boiteau R., Greaves M. and Elderfield H. (2012) Authigenic uranium in foraminiferal coatings: a proxy for ocean redox chemistry. *Paleoceanography* **27**, PA3227.

Boyle E. A. (1983) Manganese carbonate overgrowths on foraminifera tests. *Geochim. Cosmochim. Acta* **47**, 1815–1819.

Brown S. J. and Elderfield H. (1996) Variations in Mg/Ca and Sr/Ca ratios of planktonic foraminifera caused by postdepositional dissolution: Evidence of shallow Mg-dependent dissolution. *Paleoceanography* **11**, 543–551.

Bubenshchikova N., Nürnberg D., Lembke-Jene L. and Pavlova G. (2008) Living benthic foraminifera of the Okhotsk Sea: faunal composition, standing stocks and microhabitats. *Mar. Micropaleontol.* **69**, 314–333.

Cartapanis O., Bianchi D., Jaccard S. L. and Galbraith E. D. (2016) Global pulses of organic carbon burial in deep-sea sediments during glacial maxima. *Nat. Commun.* **7**, 10796.

Chen P., Yu J. and Jin Z. (2017) An evaluation of benthic foraminiferal U/Ca and U/Mn proxies for deep ocean carbonate chemistry and redox conditions. *Geochem. Geophys. Geosyst.* **18**, 617–630.

Consolaro C., Rasmussen T. L., Panieri G., Mienert J., Bünz S. and Sztybor K. (2015) Carbon isotope (δ13C) excursions suggest times of major methane release during the last 14 kyr in Fram Strait, the deep-water gateway to the Arctic. *Clim. Past* **11**, 669–685.

Cook M. S., Keigwin L. D., Birgel D. and Hinrichs K.-U. (2011) Repeated pulses of vertical methane flux recorded in glacial sediments from the southeast Bering Sea. *Paleoceanography* **26**, PA2210.

Crémière A., Pierre C., Blanc-Valleron M.-M., Zitter T., Çağatay M. N. and Henry P. (2012) Methane-derived authigenic carbonates along the North Anatolian fault system in the Sea of Marmara (Turkey). *Deep Sea Res. Part I Oceanogr. Res. Pap.* **66**, 114–130.

Cushman J. A. (1933) New Arctic Foraminifera collected by Capt. R. A. Bartlett from Fox Basin and off the northeast coast of Greenland (with two plates). *Smithson. Misc. Collect.* **89**, 1–8.

D'Hondt S., Rutherford S. and Spivack A. J. (2002) Metabolic activity of subsurface life in deep-sea sediments. *Science* **295**, 2067–2070.

Davies L. and Gather U. (1993) The identification of multiple outliers. *J. Am. Stat. Assoc.* **88**, 782.

Detlef H., Belt S. T., Sosdian S. M., Smik L., Lear C. H., Hall I. R., Cabedo-Sanz P., Husum K. and Kender S. (2018) Sea ice dynamics across the Mid-Pleistocene transition in the Bering Sea. *Nat. Commun.* **9**, 941.

Edgar K. M., Anagnostou E., Pearson P. N. and Foster G. L. (2015) Assessing the impact of diagenesis on δ 11 B, δ 13 C, δ 18 O, Sr/Ca and B/Ca values in fossil planktic foraminiferal calcite. *Geochim. Cosmochim. Acta* **166**, 189–209.

Edgar K. M., Pälike H. and Wilson P. A. (2013) Testing the impact of diagenesis on the δ^{18}O and δ^{13}C of benthic foraminiferal calcite from a sediment burial depth transect in the equatorial Pacific. *Paleoceanography* **28**, 468–480.

Elderfield H., Yu J., Anand P., Kiefer T. and Nyland B. (2006) Calibrations for benthic foraminiferal Mg/Ca paleothermometry and the carbonate ion hypothesis. *Earth Planet. Sci. Lett.* **250**, 633–649.

Erez J. (2003) The source of ions for biomineralization in foraminifera and their implications for paleoceanographic proxies. *Rev. Mineral. Geochem.* **54**, 115–149.

Evans D. and Müller W. (2018) Automated extraction of a five-year LA-ICP-MS trace element data set of ten common glass and carbonate reference materials: long-term data quality, optimisation and laser cell homogeneity. *Geostand. Geoanalytical Res.* **42**, 159–188.

Expedition 323 Scientists (2010) Bering Sea pealeoceanography: Pliocene-Pleistocene paleoceanography and climate history of the Bering Sea. *IODP Prelim. Rep.* **323**.

Froelich P. N., Klinkhammer G. P., Bender M. L., Luedtke N. A., Heath G. R., Cullen D., Dauphin P., Hammond D., Hartman B. and Maynard V. (1979) Early oxidation of organic matter in pelagic sediments of the eastern equatorial Atlantic: suboxic diagenesis. *Geochim. Cosmochim. Acta* **43**, 1075–1090.

Gottschalk J., Skinner L. C., Lippold J., Vogel H., Frank N., Jaccard S. L. and Waelbroeck C. (2016) Biological and physical controls in the Southern Ocean on past millennial-scale atmospheric CO_2 changes. *Nat. Commun.* **7**, 11539.

Groeneveld J. and Filipsson H. L. (2013) Mg/Ca and Mn/Ca ratios in benthic foraminifera: the potential to reconstruct past variations in temperature and hypoxia in shelf regions. *Biogeosciences* **10**, 5125–5138.

Gussone N., Filipsson H. L. and Kuhnert H. (2016) Mg/Ca, Sr/Ca and Ca isotope ratios in benthonic foraminifers related to test structure, mineralogy and environmental controls. *Geochim. Cosmochim. Acta* **173**, 142–159.

Hasenfratz A. P., Martínez-García A., Jaccard S. L., Vance D., Wälle M., Greaves M. and Haug G. H. (2017a) Determination of the Mg/Mn ratio in foraminiferal coatings: an approach to correct Mg/Ca temperatures for Mn-rich contaminant phases. *Earth Planet. Sci. Lett.* **457**, 335–347.

Hasenfratz A. P., Schiebel R., Thornalley D. J. R., Schönfeld J., Jaccard S. L., Martínez-García A., Holbourn A., Jennings A. E., Kuhnt W., Lear C. H., Marchitto T. M., Quillmann U., Rosenthal Y., Yu J. and Haug G. H. (2017b) Mg/Ca-temperature calibration for the benthic foraminifera Melonis barleeanum and Melonis pompilioides. *Geochim. Cosmochim. Acta* **217**, 365–383.

Hill T. M., Kennett J. P. and Spero H. J. (2003) Foraminifera as indicators of methane-rich environments: a study of modern methane seeps in Santa Barbara Channel, California. *Mar. Micropaleontol.* **49**, 123–138.

Hill T. M., Kennett J. P. and Valentine D. L. (2004) Isotopic evidence for the incorporation of methane-derived carbon into foraminifera from modern methane seeps, Hydrate Ridge, Northeast Pacific. *Geochim. Cosmochim. Acta* **68**, 4619–4627.

Hong W.-L., Torres M. E., Kim J.-H., Choi J. and Bahk J.-J. (2013) Carbon cycling within the sulfate-methane-transition-zone in marine sediments from the Ulleung Basin. *Biogeochemistry* **115**, 129–148.

Hurst M. P., Aguilar-Islas A. M. and Bruland K. W. (2010) Iron in the southeastern Bering Sea: elevated leachable particulate Fe in shelf bottom waters as an important source for surface waters. *Cont. Shelf Res.* **30**, 467–480.

Jochum K. P., Weis U., Stoll B., Kuzmin D., Yang Q., Raczek I., Jacob D. E., Stracke A., Birbaum K., Frick D. A., Günther D. and Enzweiler J. (2011) Determination of reference values for NIST SRM 610–617 glasses following ISO guidelines. *Geostand. Geoanal. Res.* **35**, 397–429.

Jonkers L., Buse B., Brummer G.-J. A. and Hall I. R. (2016) Chamber formation leads to Mg/Ca banding in the planktonic foraminifer Neogloboquadrina pachyderma. *Earth Planet. Sci. Lett.* **451**, 177–184.

Kearns S., Buse B. and Wade J. (2014) Mitigating thermal beam damage with metallic coats in low voltage FEG-EPMA of geological materials. *Microsc. Microanal.* **20**, 740–741.

Kender S., Ravelo A. C., Worne S., Swann G. E. A., Leng M. J., Asahi H., Becker J., Detlef H., Aiello I. W., Andreasen D. and Hall I. R. (2018) Closure of the Bering Strait caused mid-Pleistocene transition cooling. *Nat. Commun.* **9**, 5386.

Kim S., Takahashi K., Khim B.-K., Kanematsu Y., Asahi H. and Ravelo A. C. (2014) Biogenic opal production changes during the Mid-Pleistocene Transition in the Bering Sea (IODP Expedition 323 Site U1343). *Quat. Res.* **81**, 151–157.

Klinkhammer G. P. and Palmer M. R. (1991) Uranium in the oceans: where it goes and why. *Geochim. Cosmochim. Acta* **55**, 1799–1806.

Kristjánsdóttir G. B., Lea D. W., Jennings A. E., Pak D. K. and Belanger C. (2007) New spatial Mg/Ca-temperature calibrations for three Arctic, benthic foraminifera and reconstruction of north Iceland shelf temperature for the past 4000 years. *Geochem. Geophys. Geosyst.* **8**, Q03P21.

Ladd C., Stabeno P. J. and O'Hern J. E. (2012) Observations of a Pribilof eddy. *Deep Sea Res. Part I Oceanogr. Res. Pap.* **66**, 67–76.

Lam P. J. and Bishop J. K. B. (2008) The continental margin is a key source of iron to the HNLC North Pacific Ocean. *Geophys. Res. Lett.* **35**, L07608.

de Lange G. J., van Os B. and Poorter R. (1992) Geochemical composition and inferred accretion rates of sediments and managanese nodules from a submarine hill in the Madeira Abyssal Plain, eastern North Atlantic. *Mar. Geol.* **109**, 171–194.

Lea D. W., Pak D. K. and Paradis G. (2005) Influence of volcanic shards on foraminiferal Mg/Ca in a core from the Galápagos region. *Geochem. Geophys. Geosyst.* **6**, Q11P04.

Lear C. H., Mawbey E. M. and Rosenthal Y. (2010) Cenozoic benthic foraminiferal Mg/Ca and Li/Ca records: Toward unlocking temperatures and saturation states. *Paleoceanography* **25**, PA4215.

Lear C. H., Rosenthal Y. and Slowey N. (2002) Benthic foraminiferal Mg/Ca-paleothermometry: a revised core-top calibration. *Geochim. Cosmochim. Acta* **66**, 3375–3387.

Lehmann M. F., Sigman D. M., McCorkle D. C., Brunelle B. G., Hoffmann S., Kienast M., Cane G. and Clement J. (2005) Origin of the deep Bering Sea nitrate deficit: Constraints from the nitrogen and oxygen isotopic composition of water column nitrate and benthic nitrate fluxes. *Global Biogeochem. Cycl.* **19**, GB4005.

Lin Q., Wang J., Algeo T. J., Sun F. and Lin R. (2016) Enhanced framboidal pyrite formation related to anaerobic oxidation of methane in the sulfate-methane transition zone of the northern South China Sea. *Mar. Geol.* **379**, 100–108.

Lingling X. and Min D. (2005) Dolomite used as raw material to produce MgO-based expansive agent. *Cem. Concr. Res.* **35**, 1480–1485.

Longerich H. P., Jackson S. E. and Günther D. (1996) Inter-laboratory note. Laser ablation inductively coupled plasma mass spectrometric transient signal data acquisition and analyte concentration calculation. *J. Anal. At. Spectrom.* **11**, 899–904.

Martin P. A., Lea D. W., Rosenthal Y., Shackleton N. J., Sarnthein M. and Papenfuss T. (2002) Quaternary deep sea temperature histories derived from benthic foraminiferal Mg/Ca. *Earth Planet. Sci. Lett.* **198**, 193–209.

Martin R. A., Nesbitt E. A. and Campbell K. A. (2007) Carbon stable isotopic composition of benthic foraminifera from Pliocene cold methane seeps, Cascadia accretionary margin. *Palaeogeogr. Palaeoclimatol. Palaeoecol.* **246**, 260–277.

May T. W. and Wiedmeyer R. H. (1998) A table of polyatomic interferences in ICP-MS. *At. Spectrosc.* **19**, 150–155.

McCorkle D. C., Martin P. A., Lea D. W. and Klinkhammer G. P. (1995) Evidence of a dissolution effect on benthic foraminiferal shell chemistry: δ13C, Cd/Ca, Ba/Ca, and Sr/Ca results from the Ontong Java Plateau. *Paleoceanography* **10**, 699–714.

Millo C., Sarnthein M., Erlenkeuser H., Grootes P. M. and Andersen N. (2005) Methane-induced early diagenesis of foraminiferal tests in the southwestern Greenland Sea. *Mar. Micropaleontol.* **58**, 1–12.

Mizobata K. and Saitoh S. (2004) Variability of Bering Sea eddies and primary productivity along the shelf edge during 1998–2000 using satellite multisensor remote sensing. *J. Mar. Syst.* **50**, 101–111.

Mizobata K., Saitoh S. I., Shiomoto A., Miyamura T., Shiga N., Imai K., Toratani M., Kajiwara Y. and Sasaoka K. (2002) Bering Sea cyclonic and anticyclonic eddies observed during summer 2000 and 2001. *Prog. Oceanogr.* **55**, 65–75.

Mizobata K., Saitoh S. and Wang J. (2008) Interannual variability of summer biochemical enhancement in relation to mesoscale eddies at the shelf break in the vicinity of the Pribilof Islands, Bering Sea. *Deep Sea Res. Part II Top. Stud. Oceanogr.* **55**, 1717–1728.

Moore J. K., Doney S. C., Glover D. M. and Fung I. Y. (2001) Iron cycling and nutrient-limitation patterns in surface waters of the World Ocean. *Deep Sea Res. Part II Top. Stud. Oceanogr.* **49**, 463–507.

Mucci A. and Morse J. W. (1983) The incorporation of Mg2+ and Sr2+ into calcite overgrowths: influences of growth rate and solution composition. *Geochim. Cosmochim. Acta* **47**, 217–233.

Naehr T. H., Eichhubl P., Orphan V. J., Hovland M., Paull C. K., Ussler W., Lorenson T. D. and Greene H. G. (2007) Authigenic carbonate formation at hydrocarbon seeps in continental margin sediments: a comparative study. *Deep Sea Res. Part II Top. Stud. Oceanogr.* **54**, 1268–1291.

Nairn M. (2019) Mid-Late Miocene climate constrained by a new Laser Ablation ICP-MS set up (Ph.D. thesis). *School of Earth and Ocean Sciences*. Cardiff University.

Panieri G., Graves C. A. and James R. H. (2016) Paleo-methane emissions recorded in foraminifera near the landward limit of the gas hydrate stability zone offshore western Svalbard. *Geochem. Geophys. Geosyst.* **17**, 521–537.

Panieri G., James R. H., Camerlenghi A., Westbrook G. K., Consolaro C., Cacho I., Cesari V. and Cervera C. S. (2014) Record of methane emissions from the West Svalbard continental margin during the last 23.500 yrs revealed by δ13C of benthic foraminifera. *Glob. Planet. Change* **122**, 151–160.

Panieri G., Lepland A., Whitehouse M. J., Wirth R., Raanes M. P., James R. H., Graves C. A., Crémière A. and Schneider A. (2017) Diagenetic Mg-calcite overgrowths on foraminiferal tests in the vicinity of methane seeps. *Earth Planet. Sci. Lett.* **458**, 203–212.

Pattan J. N. (1993) Manganese micronodules: a possible indicator of sedimentary environments. *Mar. Geol.* **113**, 331–344.

Peckmann J., Reimer A., Luth U., Luth C., Hansen B., Heinicke C., Hoefs J. and Reitner J. (2001) Methane-derived carbonates and authigenic pyrite from the northwestern Black Sea. *Mar. Geol.* **177**, 129–150.

Pena L. D., Cacho I., Calvo E., Pelejero C., Eggins S. and Sadekov A. (2008) Characterization of contaminant phases in foraminifera carbonates by electron microprobe mapping. *Geochem. Geophys. Geosyst.* **9**, Q07012.

Pena L. D., Calvo E., Cacho I., Eggins S. and Pelejero C. (2005) Identification and removal of Mn-Mg-rich contaminant phases on foraminiferal tests: Implications for Mg/Ca past temperature reconstructions. *Geochem. Geophys. Geosyst.* **6**, Q09P02.

Petersen J., Barras C., Bézos A., La C., de Nooijer L. J., Meysman F. J. R., Mouret A., Slomp C. P. and Jorissen F. J. (2018) Mn/Ca intra- and inter-test variability in the benthic foraminifer Ammonia tepida. *Biogeosciences* **15**, 331–348.

Pierre C., Blanc-Valleron M.-M., Caquineau S., März C., Ravelo A. C., Takahashi K. and Alvarez Zarikian C. (2016) Mineralogical, geochemical and isotopic characterization of authigenic carbonates from the methane-bearing sediments of the Bering Sea continental margin (IODP Expedition 323, Sites U1343–U1345). *Deep Sea Res. Part II Top. Stud. Oceanogr.* **125–126**, 133–144.

Pierre C. and Fouquet Y. (2007) Authigenic carbonates from methane seeps of the Congo deep-sea fan. *Geo-Mar. Lett.* **27**, 249–257.

R Studio Team, 2015. R Studio: Integrated Development for R.

Raitzsch M., Kuhnert H., Hathorne E. C., Groeneveld J. and Bickert T. (2011) U/Ca in benthic foraminifers: a proxy for the deep-sea carbonate saturation. *Geochem. Geophys. Geosyst.* **12**, Q06019.

Rathmann S., Hess S., Kuhnert H. and Mulitza S. (2004) Mg/Ca ratios of the benthic foraminifera Oridorsalis umbonatus obtained by laser ablation from core top sediments: relationship to bottom water temperature. *Geochem. Geophys. Geosyst.* **5**, Q12013.

Roberts H. H. and Aharon P. (1994) Hydrocarbon-derived carbonate buildups of the northern Gulf of Mexico continental

slope: a review of submersible investigations. *Geo-Mar. Lett.* **14**, 135–148.

Rosenthal Y., Boyle E. A. and Slowey N. (1997) Temperature control on the incorporation of magnesium, strontium, fluorine, and cadmium into benthic foraminiferal shells from Little Bahama Bank: prospects for thermocline paleoceanography. *Geochim. Cosmochim. Acta* **61**, 3633–3643.

Rucker J. B. and Carver R. E. (1969) A survey of the carbonate mineralogy of cheilostome Bryozoa. *J. Paleontol.* **43**, 791–799.

Russell A. D., Hönisch B., Spero H. J. and Lea D. W. (2004) Effects of seawater carbonate ion concentration and temperature on shell U, Mg, and Sr in cultured planktonic foraminifera. *Geochim. Cosmochim. Acta* **68**, 4347–4361.

Saidova K. M. (1961) Ecology of foraminifera and paleogeography of the USSR FAr Eastern seas and the Northwestern Pacific: Ekologiya foraminifer i paleogeographyia dalnevostochnih morei SSSR i severo-zapadnoi chasti Tihogo okeana. *Nauka* **221**.

Schneider A., Crémière A., Panieri G., Lepland A. and Knies J. (2017) Diagenetic alteration of benthic foraminifera from a methane seep site on Vestnesa Ridge (NW Svalbard). *Deep Sea Res. Part I Oceanogr. Res. Pap.* **123**, 22–34.

Schrag D. P., Higgins J. A., Macdonald F. A. and Johnston D. T. (2013) Authigenic carbonate and the history of the global carbon cycle. *Science* **339**, 540–543.

Sexton P. F. and Wilson P. A. (2009) Preservation of benthic foraminifera and reliability of deep-sea temperature records: importance of sedimentation rates, lithology, and the need to examine test wall structure. *Paleoceanography* **24**, PA2208.

Sexton P. F., Wilson P. A. and Pearson P. N. (2006) Microstructural and geochemical perspectives on planktic foraminiferal preservation: "Glassy" versus "Frosty". *Geochem. Geophys. Geosyst.* **7**, Q12P19.

Skirbekk K., Hald M., Marchitto T. M., Junttila J., Kristensen D. K. and Sørensen S. A. (2016) Benthic foraminiferal growth seasons implied from Mg/Ca-temperature correlations for three Arctic species. *Geochem. Geophys. Geosyst.* **17**, 4684–4704.

Smith M. P. (1986) Silver coating inhibits electron microprobe beam damage of carbonates. *J. Sediment. Res.* **56**, 560–561.

Springer A. M., McRoy P. C. and Flint M. V. (1996) The Bering Sea Green Belt: shelf-edge processes and ecosystem production. *Fish. Oceanogr.* **5**, 205–223.

Sturchio N. C., Antonio M. R., Soderholm L., Sutton S. R. and Brannon J. C. (1998) Tetravalent uranium in calcite. *Science* **281**, 971–973.

Tanaka T., Yasuda I., Kuma K. and Nishioka J. (2012) Vertical turbulent iron flux sustains the Green Belt along the shelf break in the southeastern Bering Sea. *Geophys. Res. Lett.* **39**, L08603.

Teichert B. M. A., Johnson J. E., Solomon E. A., Giosan L., Rose K., Kocherla M., Connolly E. C. and Torres M. E. (2014) Composition and origin of authigenic carbonates in the Krishna-Godavari and Mahanadi Basins, eastern continental margin of India. *Mar. Pet. Geol.* **58**, 438–460.

Torres M. E., Martin R. A., Klinkhammer G. P. and Nesbitt E. A. (2010) Post depositional alteration of foraminiferal shells in cold seep settings: New insights from flow-through time-resolved analyses of biogenic and inorganic seep carbonates. *Earth Planet. Sci. Lett.* **299**, 10–22.

Ussler W. and Paull C. K. (2008) Rates of anaerobic oxidation of methane and authigenic carbonate mineralization in methane-rich deep-sea sediments inferred from models and geochemical profiles. *Earth Planet. Sci. Lett.* **266**, 271–287.

Walsh J. J., McRoy C. P., Coachman L. K., Goering J. J., Nihoul J. J., Whitledge T. E., Blackburn T. H., Parker P. L., Wirick C. D., Shuert P. G., Grebmeier J. M., Springer A. M., Tripp R. D., Hansell D. A., Djenidi S., Deleersnijder E., Henriksen K., Lund B. A., Andersen P., Müller-Karger F. E. and Dean K. (1989) Carbon and nitrogen cycling within the Bering/Chukchi Seas: source regions for organic matter effecting AOU demands of the Arctic Ocean. *Prog. Oceanogr.* **22**, 277–359.

Walter L. M. (1986) Relative efficiency of carbonate dissolution and precipitation during diagenesis: a progress report on the role of solution chemistry. In *Roles of Organic Matter in Sediment Diagenesis*. SEPM (Society for Sedimentary Geology), pp. 1–11.

Wan S., Feng D., Chen F., Zhuang C. and Chen D. (2018) Foraminifera from gas hydrate-bearing sediments of the northeastern South China Sea: proxy evaluation and application for methane release activity. *J. Asian Earth Sci.* **168**, 125–136.

Wehrmann L. M., Risgaard-Petersen N., Schrum H. N., Walsh E. A., Huh Y., Ikehara M., Pierre C., D'Hondt S., Ferdelman T. G., Ravelo A. C., Takahashi K. and Zarikian C. A. (2011) Coupled organic and inorganic carbon cycling in the deep subseafloor sediment of the northeastern Bering Sea Slope (IODP Exp. 323). *Chem. Geol.* **284**, 251–261.

Whitledge T. E. and Luchin V. A. (1999) Summary of chemical distributions and dynamics in the Bering Sea. In *Dynamics of the Bering Sea* (eds. T. R. Loughlin and K. Othani). University of Alaska Sea Grant.

Yu J., Elderfield H., Greaves M. and Day J. (2007) Preferential dissolution of benthic foraminiferal calcite during laboratory reductive cleaning. *Geochem. Geophys. Geosyst.* **8**, Q06016.

Zhao M.-Y., Zheng Y.-F. and Zhao Y.-Y. (2016) Seeking a geochemical identifier for authigenic carbonate. *Nat. Commun.* **7**, 10885.

Associate editor: Thomas M. Marchitto